**High-Fidelity Time-Series Data Synthesis based on Finite Element Simulation and Data Space Projection**

Youqi Zhang[a,*], Zhenkun Li[a], Rui Hao[a], Weiwei Lin[a], Lingfang Li[b], and Di Su[c]

[a] *Department of Civil Engineering, School of Engineering, Aalto University, Espoo, Finland*

[b] *Department of Civil and Environmental Engineering, The Hong Kong Polytechnic University, Hong Kong, China*

[c] *Department of Civil Engineering, The University of Tokyo, Tokyo, Japan*

[*] Corresponding author: Email: youqi.zhang@aalto.fi

**Abstract:** Dynamic responses can provide rich information for supporting the entire life cycle of structures, and they can either be measured from actual structures or simulated using the finite element (FE) method. For the FE simulation, insufficient fidelity of simulation data can significantly affect the confidence of analysis results, while FE model updating methods can partially address this problem by reducing the simulation error. However, most FE model updating methods inevitably update the hyperparameters of FE models using sophisticated algorithms with high computational complexities. Thus, one question was raised: whether there is a projection that can transfer the FE simulation data to the corresponding measurement data directly without performing FE model updating? To achieve this, we proposed a data synthesis method using FE simulation and deep learning space projection, which can be used to synthesize high-fidelity dynamic responses excited by some unseen load patterns in the measurement. A Dilated Causal Convolutional Neural Network (DCCNN) was designed for realising the space projection. Vibration experiments were conducted on both an I-shaped steel beam and the corresponding FE model to establish datasets and test the proposed method. The quality of the synthetic data was analysed in both the time domain and the frequency domain. The accurate amplitudes, natural frequencies, and mode shapes of the synthetic data successfully demonstrate the effectiveness of the proposed high-fidelity data synthesis method.

**Keywords:** data synthesis, finite element analysis, space projection, Dilated Causal Convolutional Neural Network

## 1. Introduction

Measurement data of dynamic behaviours is fundamental for supporting the entire life cycle of structures, which includes design optimization [1, 2], analysis of structural behaviours [3-9], health assessment, damage prognostics [10-12], development of analytical methods [13, 14], etc. Powered by advanced sensing technology and structural health monitoring (SHM) systems [15], dynamic structure behaviours can be observed, and the corresponding measurement data can be acquired. However, in many engineering scenarios, it is challenging or even impossible to acquire measurement data from structures [16, 17]. To address this challenge, finite element (FE) models are widely used for simulating structural dynamics and analysing structural performance. One crucial factor that affects the results of analyses is the quality or fidelity of simulation data. Indeed, deviations between the FE simulation data and the measured dynamic responses of real structures are inevitable [18], and the insufficient fidelity of simulation data can greatly affect the confidence of analysis results.

The reasons for the deviations between FE simulation and measurement data mainly consist of three perspectives. Firstly, FE simulation is based on many assumptions and approximations [19-21], for instance, constant axial stiffness *EA* and the transition from continuum to discrete. It is impossible to consider all the properties of structures and model them accurately, resulting in inevitable modelling deviations. Secondly, measurements of actual structures involve enormous uncertainties and random processes [22, 23], such as boundary conditions and noise, which are difficult to be modelled accurately. Thirdly, as sensor systems are not perfect, measurement error appears in all the observation data [24, 25], which also increases the difference between FE simulation data and measurement data. Consequently, time-series data generated by FE simulation and measurement data are not in the identical data space.

FE model updating methods [26-28] can partially address the problem as aforementioned. FE model updating methods aim to minimize the deviation between FE models and actual structures. Typical FE model updating methods include mode-based updating methods [18, 29, 30], Bayesian methods [31-33], sensitivity-based updating methods [34, 35], frequency-based updating methods [36, 37], and machine learning-based methods [38-41], etc. Most of the existing FE model updating methods align the dominant frequency features or modal features of the FE models with the actual structures. However, most model updating methods inevitably update the hyperparameters of FE models using sophisticated algorithms with high computational complexities, and it is still challenging to simulate "high-fidelity" complex dynamic responses even using the updated FE models. One example is the simulation of structural dynamics using FE analysis. Comparing the FE simulation data of vibration to the measurement data in a short period or in the dB-scale frequency domain, apparent differences tend to be observed. Although the FE model updating methods can align the natural frequencies of the FE models to the actual structures, damping modelling can also greatly influence the fidelity of simulation data. Because of the high complexity of damping mechanism, it is challenging to model damping accurately in real engineering scenarios. Rayleigh damping, as one of the most widely adopted damping modelling methods, combines mass-proportional damping and stiffness-proportional damping. However, it does not consider the energy dissipation of friction in supports, sound emission, anchor losses, or even thermoelastic damping, resulting in some possible loss of fidelity in the simulation of structural dynamics. Therefore, simulation data generated by numerical methods are prone to be in different data space from that of measurement data. Hence, there is a need to further minimize the deviation between the data spaces of FE simulation and measurement data for improving the quality of the FE simulation data. This problem can be considered as a space projection task, which targets to project the data from the simulation data space to the measurement data space. Such data space projection can be achieved using modelling methods like Deep Learning (DL) [42] in an end-to-end manner.

DL has made a great wave of data-driven methods since 2015 [43], and it is becoming increasingly prevalent in the engineering field. Different from the traditional knowledge-based modelling approaches, DL is a data-driven method which can be applied with zero domain knowledge. Correlations between two datasets can be built automatically or projections between two different data spaces can be established automatically by training DL models. Countless examples of DL applications demonstrate DL's power in solving real-world engineering problems, for instance, SHM [16, 44-46], especially image-based structural damage detection [47-49] and vibration-based structural state identification [50-52], detection of structural components [53], etc. Meanwhile, DL has also been used for style transfer tasks in the image processing and audio processing fields. Therefore, DL has demonstrated its merits for data transfer tasks or modelling complex projection between two datasets, and has shown a full potential to achieve the projection from the simulation data space to the measurement data space.

In this article, we proposed a method to generate high-fidelity time-series synthetic data. Projections from the FE simulation data space to the measurement data space are built using DL. To the best of our knowledge, this is the first attempt to synthesize time-series data using FE simulation and DL space projection. The projection enables a significant quality improvement of the time-series simulation data without performing FE model updating. One suitable application scenario for the proposed method is that, when dynamic responses of structures excited by some unseen load patterns are not available in the real world, the proposed method can achieve high-fidelity synthetic data in an end-to-end manner. Moreover, the high-fidelity time-series synthetic data generated by the proposed method can benefit all the downstream tasks as mentioned in the first paragraph. As a reminder, this article is organized into 5 sections. After introducing the background in Section 1, the proposed data synthesis method is presented in Section 2. Then Section 3 describes the experiments and datasets, and Section 4 discusses the results. Finally, some conclusions are drawn in Section 5. This idea was initialized in a short conference paper [54], in which we briefly proved the concept using a fully-connected neural network. In this manuscript, we proposed a new light-weighted DL model with much fewer trainable parameters, tested the performance of the method more rationally, investigated the case with both sufficient and limited training data, performed quantitative analyses in both time and frequency domains, and evaluated the quality of synthetic data with modal analyses.

## 2. Methodology

### *2.1. Workflow of the proposed method*

The proposed method for time-series data synthesis is illustrated in Fig. 1. It consists of physical experiment, FE simulation, and data space projection. Identical external loads are attempted to be applied on both the actual specimen and the FE model. Even though the measurement errors of load amplitudes and manual errors of impact locations are inevitable, the errors of impact forces and locations can be managed in limited ranges. These errors are considered in the process of the proposed method which can provide some robustness to the space projection model. To prove the concept of the proposed method, vibration experiments with only hammer impact loads were performed on both a physical specimen and the corresponding numerical model. Actuators can also be used to apply excitations on structures because they can apply the assigned loads on the structures with other load patterns.

The dynamic behaviour of the physical specimen is measured using an acceleration sensor system, and the corresponding dynamic behaviour of the numerical model is simulated using FE analysis. Then a paired dataset of measurement data and FE simulation data can be obtained which are used for training, validating, and testing the DL models. Finally, a projection from the data space of the FE simulation to the data space of the measurement data is established by DL modelling. The FE simulation dataset is used as input for the DL model, and the measurement dataset is for the ground truth. Consequently, the synthetic data can be predicted by the DL model.

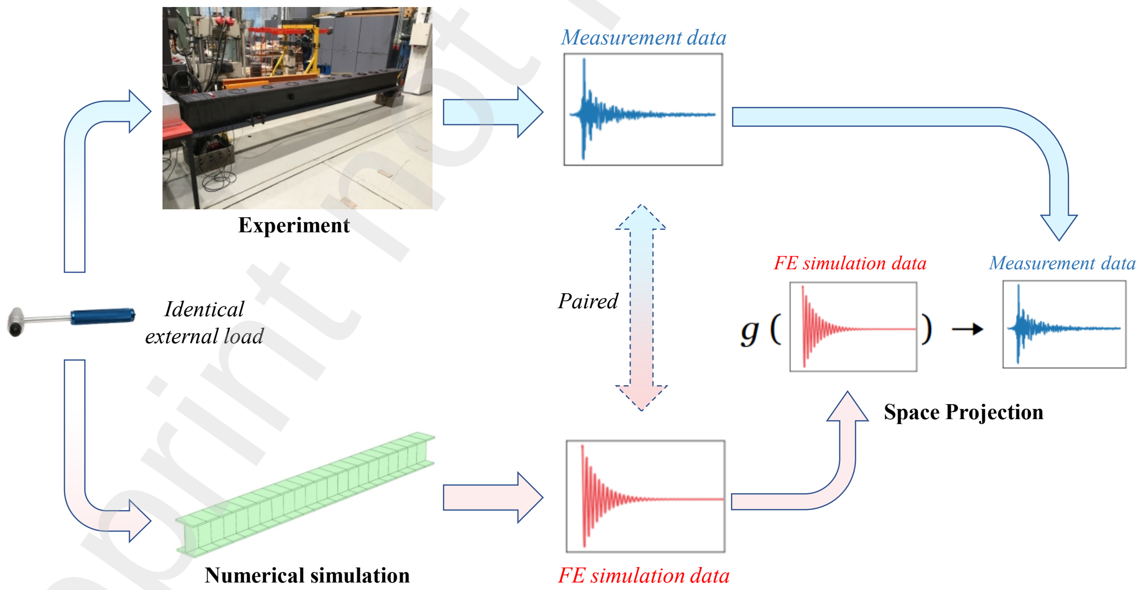


**Fig. 1.** Architecture of the proposed method for time-series data synthesis

### *2.2. DL modelling*

DL is a prevalent data-driven modelling method. It can approximate correlations between two datasets through a training procedure, with no requirement for domain knowledge. After designing the architecture of the DL model according to the specific tasks, the training process can be realised in three steps. Firstly, training data are fed into the DL model, and then corresponding predictions are obtained. Secondly, modelling loss is calculated by comparing the predictions and the ground truth via a certain loss function, e.g., mean square error (MSE). Finally, the loss is minimised using back-propagation [55] and gradient descent.

The task of DL in the proposed method is to transfer the vibration data from the simulation space to the measurement space as illustrated in Fig. 1. As this is a time-series data processing, we designed a Dilated Causal Convolutional Neural Network (DCCNN), which stacks multiple Dilated Causal Convolution (DCC) layers as its core components.

DCC is a specific type of convolution. Compared to the ordinary 1-D convolution, DCC has the operation of dilation and causal constraint. Dilation describes how convolutional kernels slide on the input data. The kernels are applied on an area that is larger than the kernel size by skipping input values with a certain step. The skipped step is called dilation rate. Stacking a few Dilated Convolution layers can effectively expand the receptive field. Causal constraint makes the prediction not depend on any neuron in the future timesteps. Such a feature makes it feasible for real-time processing, which provides a great potential of DCCNNs for being integrated into SHM systems or digital twin systems in the future. Fig. 2 shows an example of a DCCNN which includes 3 DCC layers with dilation rates of 1, 2, and 4. The receptive field reaches 16 for each neuron in the output layer in the illustration. Based on the unique characteristics of DCC, it is widely used for processing temporal data, e.g., audio generation [56], speech denoising [57], speech synthesis [58], etc. Since audio signal is a specific type of vibration data collected by microphones, it shares high similarities with the vibration data acquired from structures. Therefore, a DCCNN is proposed for time-series data synthesis.

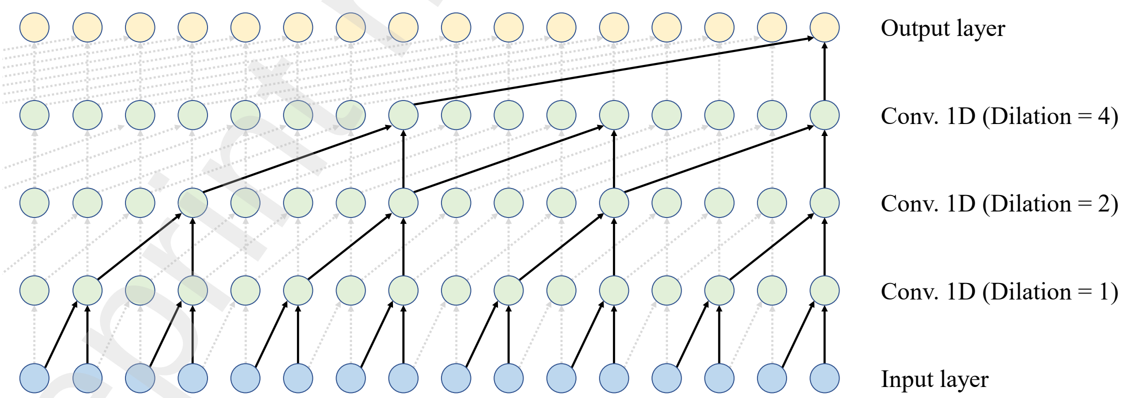


**Fig. 2.** Example of a DCCNN

The structure of the proposed DCCNN is shown in Fig. 3. In total 8 DCC layers and 8 Leaky Rectified Linear Unit (ReLU) layers are designed between the input layer and the output layer. The dilation rates are $2^i$ ($i = 0,\cdots, 7$) in the DCC layers. The number of kernels is 32 and the kernel length is 5. As a result, the receptive field for each value in the prediction is 512, which is 12.8% (512/4000) of the total data length. The number of DCC layers was determined by balancing the receptive field and the number of trainable parameters with several rounds of trial and error. Insufficient receptive fields tend to cause very low amplitudes in the latter part of the synthetic data. Long receptive fields request deep network architecture with more trainable parameters, which is computationally costly. Leaky ReLU activation function, as explained in Fig. 4, is designed after each DCC layer to induce nonlinearity in the representation of the network, where $\alpha$ of 0.5 is used to represent the negative slope.

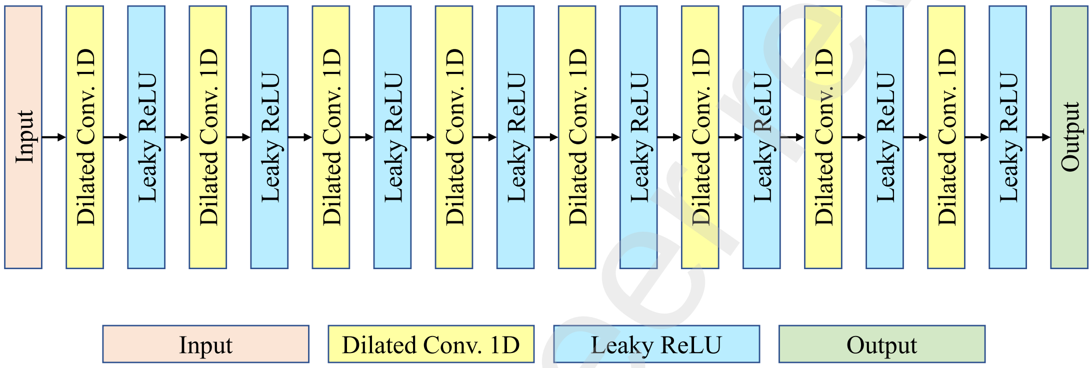


**Fig. 3.** Structure of the proposed DCCNN

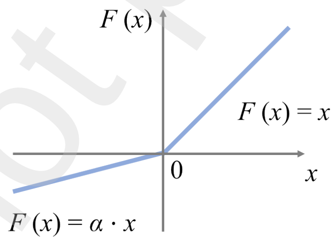


**Fig. 4.** Illustration of Leaky ReLU

Detailed parameters of the DCCNN are summarized in Table 1. The total number of trainable parameters is only 37,833, which is very close to the number of samples in each datum 36,000 (4000 samples × 9 channels). Designing similar numbers of trainable parameters in the DCCNN as the number of data samples aims to prevent over-fitting.

**Table 1.** Parameters of the DCCNN

| Layer | Output shape | Parameter | Number of Parameters |
|---|---|---|---|
| Input | 4000×9 | - | 0 |
| Conv1D_1 | 4000×32 | Dilation rate = 1 | 1472 |
| Leaky ReLU | 4000×32 | $\alpha = 0.5$ | 0 |
| Conv1D_2 | 4000×32 | Dilation rate = 2 | 5152 |
| Leaky ReLU | 4000×32 | $\alpha = 0.5$ | 0 |
| Conv1D_3 | 4000×32 | Dilation rate = 4 | 5152 |
| Leaky ReLU | 4000×32 | $\alpha = 0.5$ | 0 |
| Conv1D_4 | 4000×32 | Dilation rate = 8 | 5152 |
| Leaky ReLU | 4000×32 | $\alpha = 0.5$ | 0 |
| Conv1D_5 | 4000×32 | Dilation rate = 16 | 5152 |
| Leaky ReLU | 4000×32 | $\alpha = 0.5$ | 0 |
| Conv1D_6 | 4000×32 | Dilation rate = 32 | 5152 |
| Leaky ReLU | 4000×32 | $\alpha = 0.5$ | 0 |
| Conv1D_7 | 4000×32 | Dilation rate = 64 | 5152 |
| Leaky ReLU | 4000×32 | $\alpha = 0.5$ | 0 |
| Conv1D_8 | 4000×32 | Dilation rate = 128 | 5152 |
| Leaky ReLU | 4000×32 | $\alpha = 0.5$ | 0 |
| Output | 4000×9 | | 297 |
| ***In total*** | - | | ***37,833*** |

## 3. Experiment

As vibration data is one of the representative types of time-series data, we designed an experiment which uses vibration data to validate the proposed time-series data synthetic method. As introduced in Section 2, the proposed method comprises three main parts: physical experiment, FE simulation, and space projection. The details of those three parts in the case studies are introduced in the following subsections, respectively.

### *3.1. Physical experiment*

Figs. 5 and 6 show the layout of the physical experiment for establishing the measurement dataset of vibration data. An I-shaped steel beam was selected as the specimen owing to its moderate complexity as a real structure. The total length of the beam is 4.4 m, and the span length is 4.0 m. The beam was simply supported at its two ends, and the imperfect boundary conditions increased the uncertainties in the vibration data.

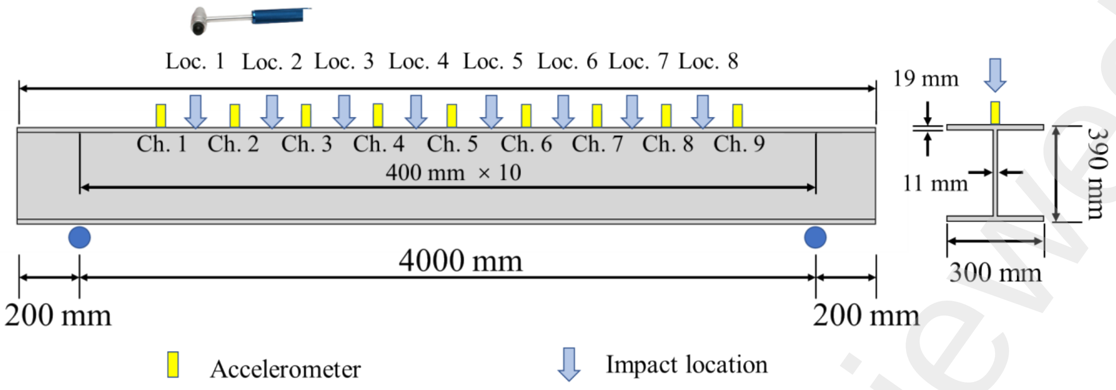


**Fig. 5.** Locations of accelerometers and hammer impacts

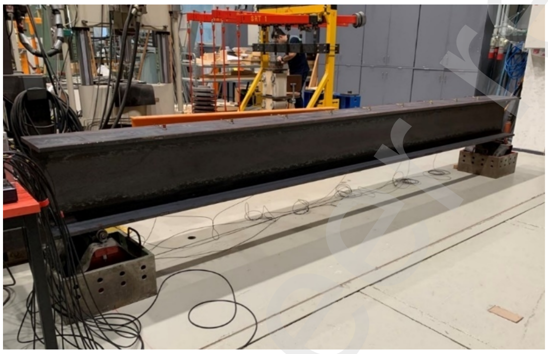

**Fig. 6.** Specimen of the vibration experiment

The vibration measurement system consists of Brüel & Kjær 4371 accelerometers, Brüel & Kjær 2635 amplifiers, an electric hammer, a Measurement Computing DT9834 multifunction USB data acquisition (DAQ) device, and a laptop computer. In total 9 accelerometers were evenly distributed on the upper flange of the beam, named from Ch. 1 to Ch. 9. The sampling frequency is 2000 Hz, and the measurement time after each hammering is 2.0 s. Thus, the vibration data of each measurement has a shape of 4000 samples × 9 channels. The measurement time of 2.0 s was determined according to the time for a free-damped vibration of the structure to vanish. Observing the variation of amplitudes of the free-damped vibration of the beam, it takes about 1.0 s from starting to the approximate end. Thus, doubling the time length of free damped vibration, 2.0 s was used to ensure sufficient information to be included in the measurement data. An electric hammer was used to measure the impact force, which triggers the measurement of free-damped vibration.

The impact locations are in the midpoint of every two adjacent accelerometers. In total, the hammer impact loads were applied on 8 locations, termed from Loc. 1 to Loc. 8. The impact forces are random and generally lower than 10 N. Examples of a hammer impact force and the corresponding response of the beam are shown in Fig. 7. The impact location is Loc. 1, and the vibration measured in Ch. 6 is shown in Fig. 7b. Because the I-beam is modelled as a structure with multiple degrees of freedom, the vibration of the beam can be considered as the superposition of multiple vibration modes. Additionally, the imperfect boundary conditions on the supports also increase the complexity of the vibration. Therefore, Fig. 7b does not show a curve with monotonically decreasing amplitudes. The numbers of hammerings in all locations are summarized in Table 2. Over 140 times of impact were applied at each location. In total, 1277 free-damped vibration data were acquired. The measurement data also contain the noise components caused by the laboratory environment, for instance, the noise of load test, electric saw cutting, moving and dropping of heavy materials, etc. Raw measurement data was used directly without any noise reduction or pre-processing.

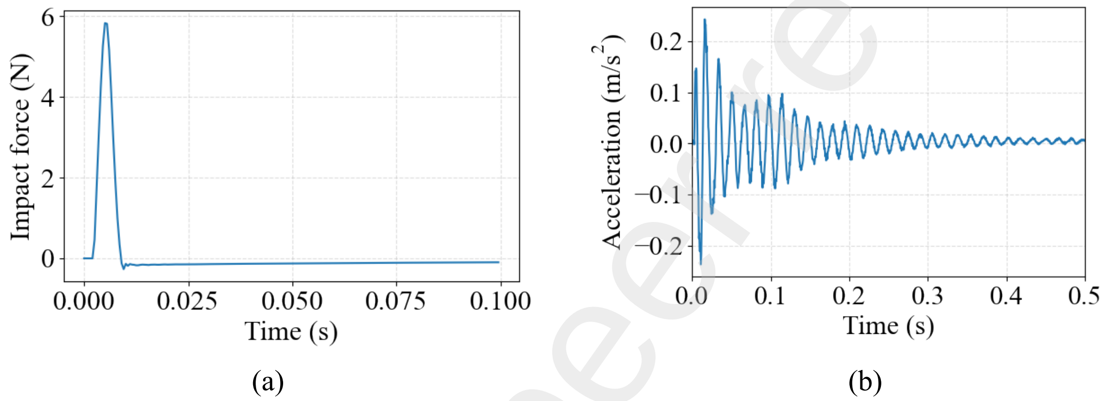


**Fig. 7.** Examples of hammer impact load and measured vibration. (a) impact load at Loc. 1, (b) measurement data of beam vibration (Ch. 6)

**Table 2.** Data distribution

| Impact location | 1 | 2 | 3 | 4 | 5 | 6 | 7 | 8 | In total |
|---|---|---|---|---|---|---|---|---|---|
| Number of data | 201 | 218 | 145 | 143 | 142 | 143 | 142 | 143 | 1,277 |

### ***3.2. FE simulation***

To build the simulation dataset and test the proposed data synthesis method, a FE model of the steel beam was established using ABAQUS, as shown in Fig. 8. We intentionally created a FE model with high modelling error or misspecification in the following ways to check whether the proposed method can yield a satisfactory result even with inaccurate modelling. First, the FE model consists of only 22 beam elements (B31) and 23 nodes. The length of each element is 0.20 m. The beam is simply supported with a span length of 4.0 m. The FE model with limited details is prone to inaccurate solutions. Second, no model updating or calibration was performed on the FE model. The model parameters, such as Young's modulus of 210 GPa, Poisson ratio of 0.3, density of 7850 kg/m$^3$, and boundary conditions of a simply-supported beam, were not calibrated to match the experimental results. Third, the Rayleigh damping factors $\alpha$ and $\beta$ in the FE model were empirically assigned $\alpha$

of $2\times10^{-3}$ and $\beta$ of $5\times10^{-5}$, respectively Those two parameters were not aligned with the damping ratios of the physical specimen calculated from the measurement data. Overall, the deviations between the physical specimen and the FE model were created deliberately with high misspecification for testing purposes.

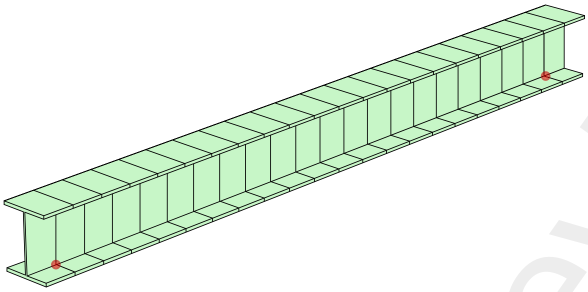

**Fig. 8.** Finite element model of the beam

The method for modelling the structural dynamics of the beam was mode superposition , which superimposes the weighted displacement of each mode shape, as shown in the examples [59, 60]. This experiment considered the superposition of the first 30 modes, which include vertical modes, horizontal modes, and longitudinal modes. As only vertical vibration is measured and discussed, only the vertical modes involved in the mode superposition are shown in Fig. 9, which are the first 4 orders of bending modes.

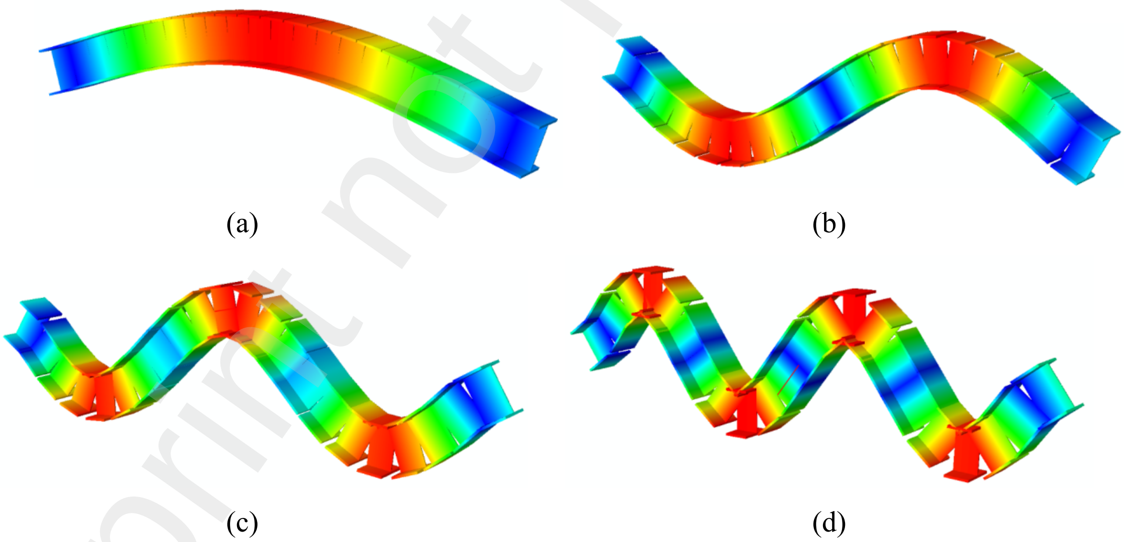


**Fig. 9.** Vertical bending modes of the FE model with natural frequencies of 80.49 Hz, 280.08 Hz, 534.13 Hz, and 840.93 Hz

The impact loads recorded in the vibration experiment were applied to the corresponding locations of the FE model. As a result, 1277 simulation data were obtained as the pairs of the corresponding measurement data. Fig. 10 shows an example of the simulation data (vibration at Ch.

6, hammer impact at Loc. 1 with the load shown in Fig. 7a). Different from its corresponding measurement data shown in Fig. 7b, the simulation data have a higher frequency, and the amplitudes of the simulation data decrease monotonically according to the prescribed Rayleigh damping.

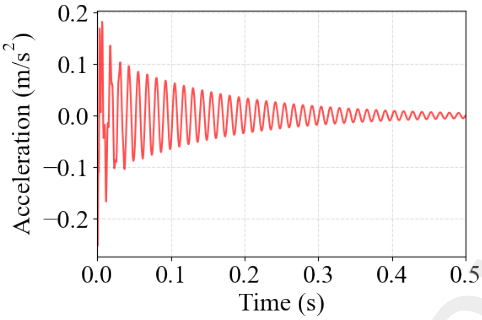


**Fig. 10.** Example of FE simulation data (Ch. 6, impact at Loc. 1)

Another detailed comparison between the measurement and simulation data in both time and frequency domains is shown in Fig. 11. The data are the vibration at Ch. 8 excited by the hammer impact at Loc. 8. In the time domain, the apparent differences in natural frequencies, amplitudes, and phases are qualitatively displayed. In the frequency domain, the difference in natural frequencies can be quantitively analysed, as summarized in Table 3. Observing the natural frequencies and damping ratios in Table 1, the differences between the measurement and simulation data can even reach 153.8%. Note that, no FE model updating was performed to minimize these differences, because we intended to investigate whether the proposed data synthesis method requests a precise FE model, or whether the proposed method can have great performance with a highly inaccurate FE model.

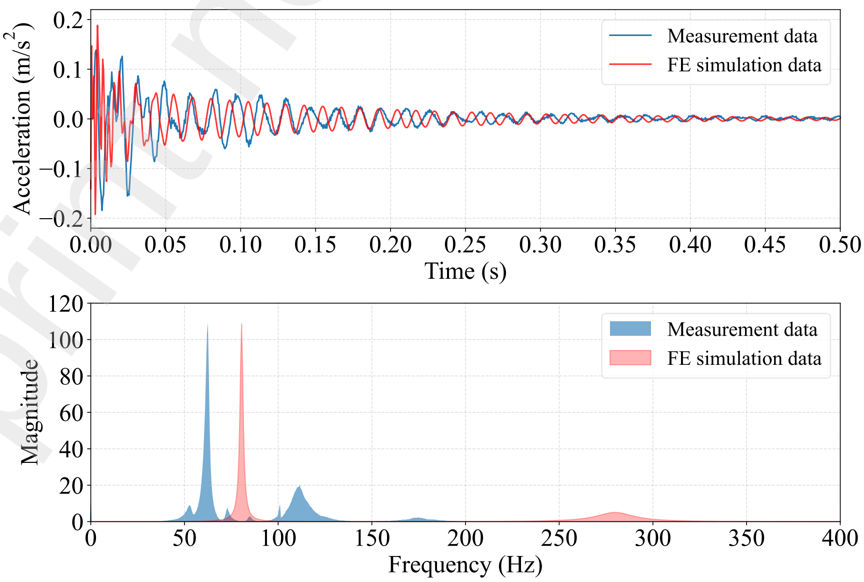


**Fig. 11.** Comparison between the measurement data and FE simulation data (Impact at Loc. 8, Ch. 8)

**Table 3.** Comparison between dynamic characteristics of the measurement and simulation data shown in Fig. 11

| Mode | Natural Frequency (Meas.) | Natural Frequency (Sim.) | Difference (ratio) | Damping Ratio (Meas.) | Damping Ratio (Sim.) | Difference (ratio) |
|---|---|---|---|---|---|---|
| 1 | 62.5 Hz | 80.5 Hz | 18 Hz (28.8%) | 2.15% | 1.26% | 0.89% (41.4%) |
| 2 | 110.5 Hz | 280.5 Hz | 170 Hz (153.8%) | 4.42% | 4.39% | 0.03% (0.68%) |

### *3.3. Network training scenarios*

Two training cases are tested for the proposed DCCNN with different amounts of training and validation data, as shown in Table 4. Case 1 is the scenario with sufficient training data, and Case 2 represents the scenario when only limited training data are available. In both cases, the vibration data excited by the impact loads at Locs. 5-8 were only used for test purposes. The difference between the two cases is the amount of training and validation data: Case 1 uses the data excited by the impact loads at Locs. 1-4 for training and validation, while Case 2 uses the data excited by the impact loads at only Loc. 1. The reason for choosing the data with impact only at Loc. 1 in Case 2 is that the impact loads near supports may lead to more complex vibration than the impacting other places. The numbers of training data in the two cases differ 3.5 times. The data split in Case 1 is used for the determination of the structure of the DCCNN, and Case 2 is for testing the performance of the DCCNN with limited training data.

**Table 4.** Data split in each case

| Case | Number of training data | Ratio (%) | Number of validation data | Ratio (%) | Number of test data | Ratio (%) |
|---|---|---|---|---|---|---|
| 1 | 636 (Locs. 1-4) | 49.8 | 71 (Locs. 1-4) | 5.6 | 570 (Locs. 5-8) | 44.6 |
| 2 | 180 (Loc. 1) | 23.4 | 21 (Loc. 1) | 2.7 | 570 (Locs. 5-8) | 73.9 |

The optimizer is Adam [61] and the loss function is MSE as defined in Eq. (1). All the DCCNNs were trained for 5000 epochs. The learning rate was initialized with 0.001, and the learning rate was scaled by a factor of 0.75 if the training loss did not reduce in 50 epochs. The results of Cases 1 and 2 are analysed and discussed in Section 4.

$$MSE = \frac{1}{n}\sum_{i=1}^{n}\left(y_i - y_i'\right)^2 \tag{1}$$

## 4. Results

This section discusses the results of data synthesis generated by the proposed DCCNN in the two training cases. By performing the vibration experiment and the FE simulation as introduced in

Section 3, two paired datasets, named measurement dataset and FE simulation dataset, are established for training, validating, and testing the proposed data synthesis method.

### *4.1. Results of Case 1*

As introduced in Table 5, the data with hammer impact at Locs. 1-4 were utilized for training and validation, and the rest data with hammer impact at Locs. 5-8 were used for testing. Fig. 12 shows the training procedures of the proposed DCCNN. Both training and validation losses decreased smoothly, and very low training and validation losses were finally achieved. No overfitting occurred during the training procedure.

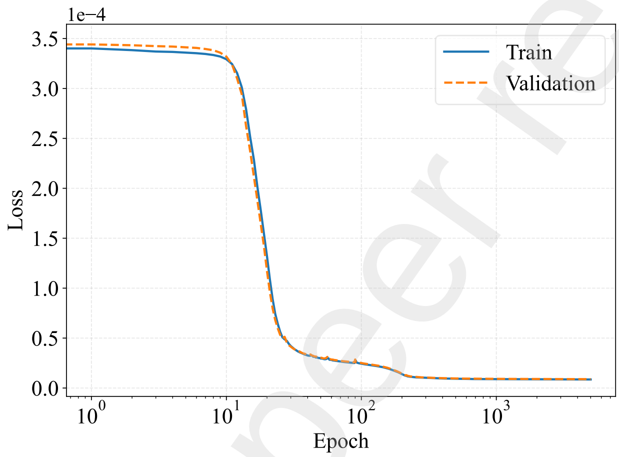


**Fig. 12.** Training history of Cases 1

To test the performance of the DCCNN model, the MSE of each test result is visualized in Fig. 13, which calculates the MSE between the measurement data (ground truth) and the synthetic data generated by the DCCNN. The MSE of each individual test data is in a range between 0.002 to 0.014, and the mean MSE is 0.006 for the whole test set, which exhibits the high fidelity of the synthetic data. The test data can be divided into 4 groups according to their impact locations (Locs. 5-8) by using different colours. Fig. 13 shows a phenomenon that, with relatively sufficient training data, the synthetic vibration data excited by the impact loads, that are close to the midpoint of the beam, tend to yield higher accuracy. In contrast, the synthetic vibration data excited by the impact loads, that are near to supports of the beam, tend to show a higher error. One possible reason for this phenomenon is the imperfect boundary conditions of the beam. When the impact load gets closer to the supports of the beam, the vibration tends to be more complex. As a result, the DCCNN is relatively more difficult to learn the features for synthetic data when the impact loads are close to the supports.

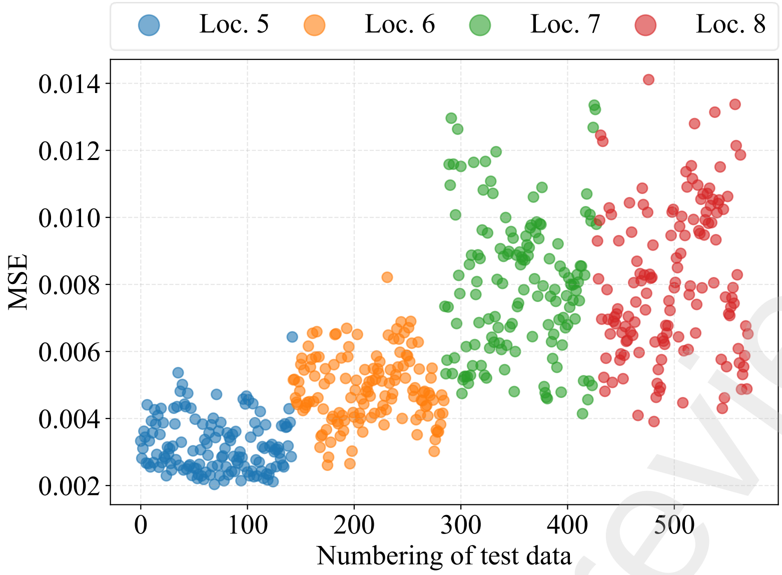


**Fig. 13.** MSE of each test data in Case 1 with the mean value of 0.006

Figs. 14 and 15 demonstrate the test result of the synthetic data generated by the proposed DCCNN in the Case 1 training scenario. Two data examples, which have lower and higher MSEs than the mean MSE of the whole test set 0.006, are randomly chosen from the test set. The first example shown in Fig. 14 is excited by an impact load at Loc. 5, and its MSE is 0.0034. The second example shown in Fig. 15 is excited by an impact load at Loc. 8, and the corresponding MSE is 0.0066. In the two figures, all 9 channels of the synthetic data and the corresponding measurement data are compared individually. In Fig. 14 the amplitude, phase, and frequency of the synthetic data precisely match the measurement data. In Fig. 15, the amplitudes of the first several periods of the synthetic data can be slightly lower than that of the measurement data. The frequency and phase are presented correctly. The results demonstrate that the proposed method can successfully synthesize the vibration data excited by the loads that are not involved in the training and validation process.

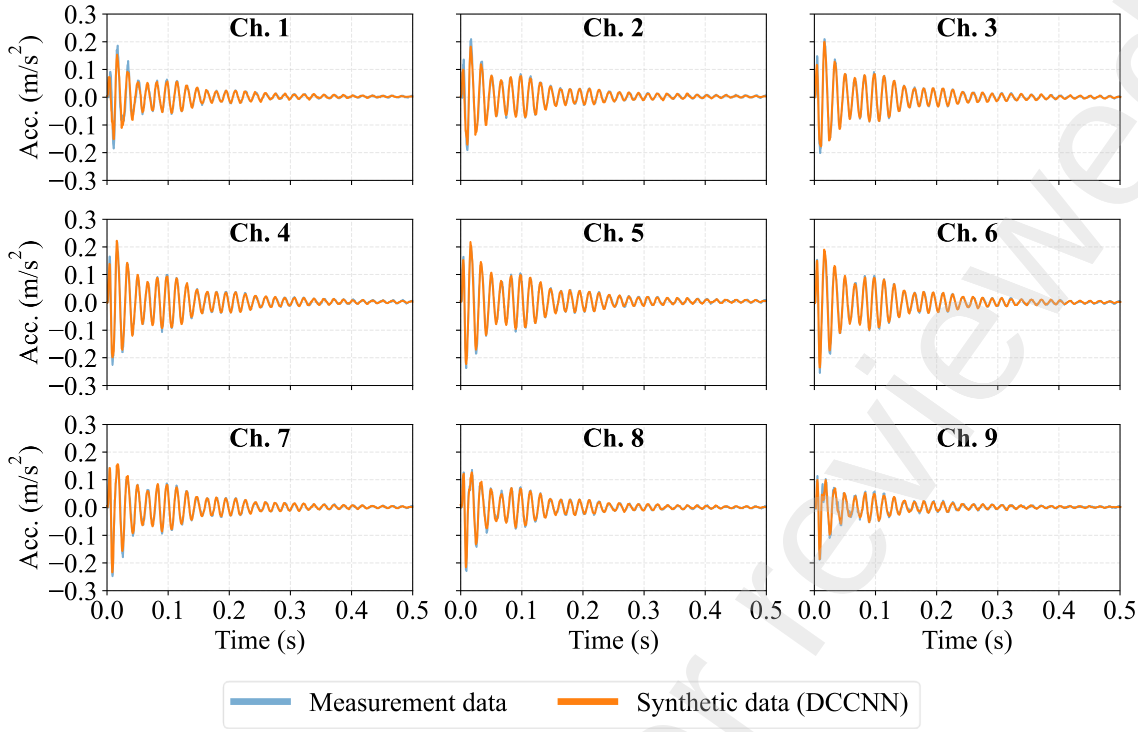


**Fig. 14.** Synthetic data generated by DCCNN (Case 1, impact on Loc. 5, MSE of 0.0034)

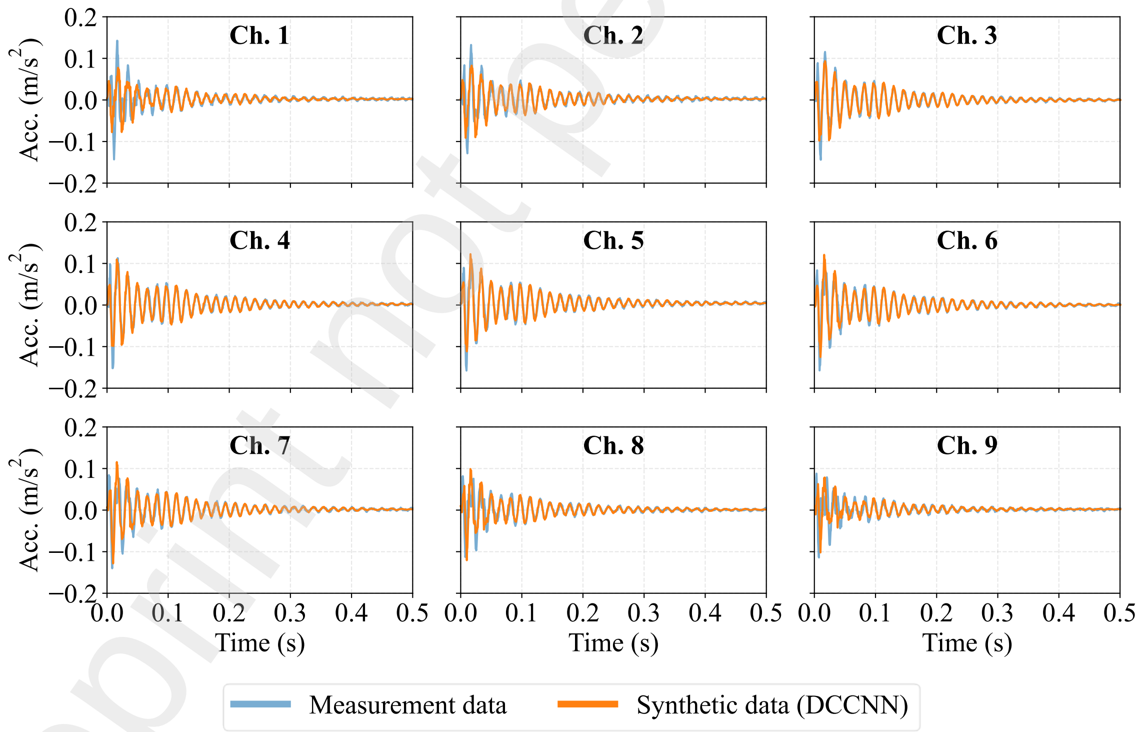


**Fig. 15.** Synthetic data generated by DCCNN (Case 1, impact at Loc.8, MSE of 0.0066)

To view more details of the synthetic data, Fig. 16 visualises the first 0.1 s of Ch. 5 in Fig. 14. Comparing the synthetic data and the corresponding measurement data (ground truth), the synthetic data precisely represent the low-frequency components of the measurement data. The difference in the high-frequency components between the measurement and synthetic data can be observed. The waveform of the measurement data has apparent sawteeth, but the waveform of the DCCNN synthesised data is smoother, indicating fewer high-frequency components in the synthetic data. Such a characteristic of DCCNN makes it feasible to have the additional function of a smoother or low-pass filter.

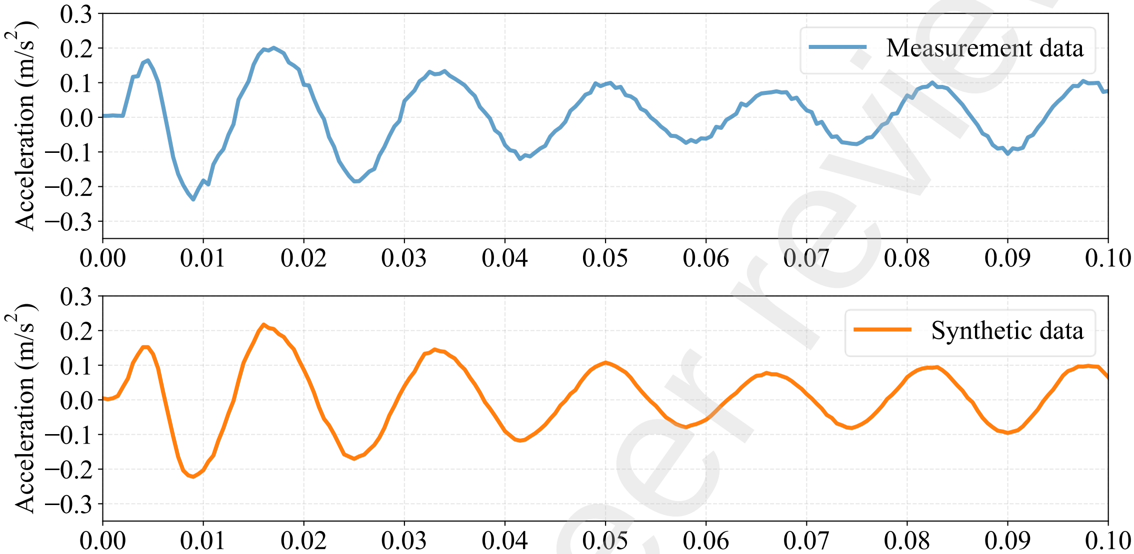


**Fig. 16.** First 0.1 s of the Ch. 5 in the synthetic data shown in Fig. 14

Subsequently, to investigate the quality of the synthetic data from the frequency perspective, we performed Fast Fourier Transformation (FFT) on the FE simulation, measurement, and synthetic data. Ch. 9 of the example (shown in Fig. 14) was visualised in Fig. 17. The subplots in the first row are the time-series waveforms, the subplots in the second row are the FFT spectrums in a linear scale, and the subplots in the last row are the FFT spectrums in the dB scale. From the linear-scale spectrums of the measurement data and synthetic data, two dominant peaks at 62.5 Hz and 110.5 Hz can be detected, indicating accurate representations of the natural modes of the beam in the synthetic data. In the dB-scale spectrum of synthetic data, the magnitudes over 200 Hz are lower than the corresponding measurement data, which proves that DCCNN has the characteristics of low-pass filter, and the components higher than about 200 Hz are depressed.

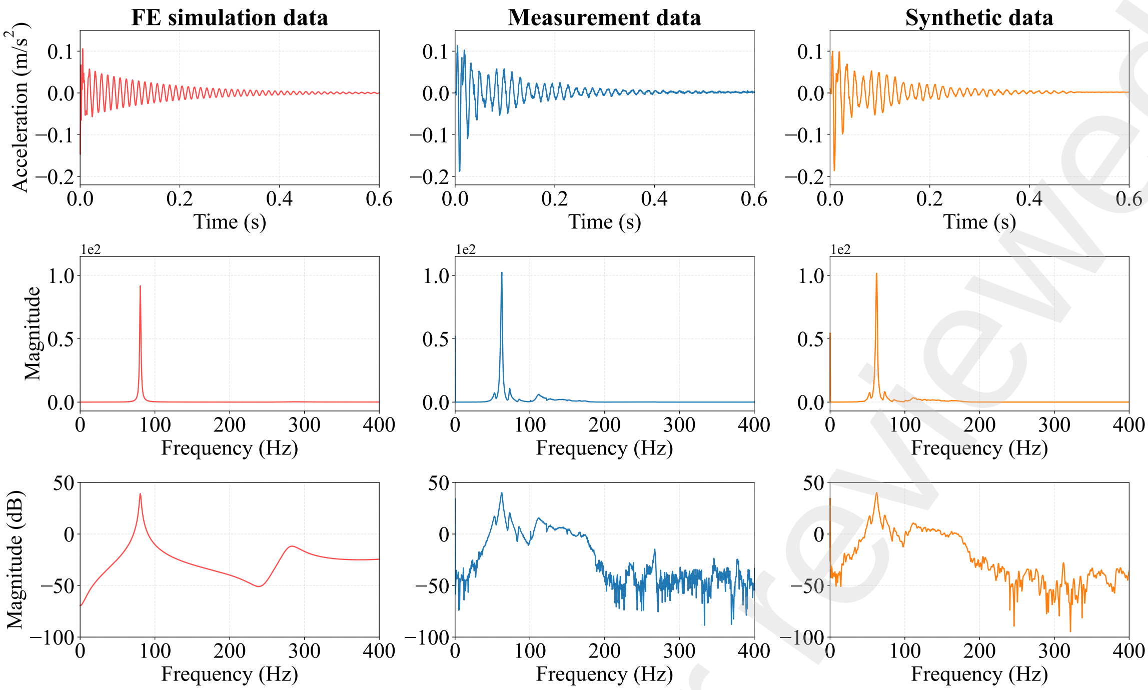


**Fig. 17.** Comparison of FE simulation, measurement, and synthetic data in the frequency domain (impact at Loc. 5, Ch. 9 of the data example in Fig. 14)

Furthermore, the mode shapes of the first two bending modes are identified from each synthetic and measurement data in the test set using cross spectrum method. The mean mode shapes of the test set data are calculated and visualised in Fig. 18, in which the mean mode shapes identified from the synthetic data are highly consistent with those of the measurement data. Even though the measured mode shapes are apparently different from simulation results, the proposed DCCNN can accurately reproduce the mode shape information in the synthetic data. Modal Assurance Criterion (MAC), as defined in Eq. (2), is used as an indicator to quantitively evaluate the accuracy of the mode shapes identified from the synthetic data. The MACs of the synthetic, FE simulation, and measurement data are analysed and visualized in Fig. 19. Overall, the MAC values of the mean mode shapes identified from the synthetic data are greater than 0.9742 compared to those of the measurement data, indicating the high quality of the synthetic data generated by the DCCNN.

$$MAC(\varphi_A,\varphi_B) = \frac{|\{\varphi_A\}^T\{\varphi_B\}|^2}{(\{\varphi_A\}^T\{\varphi_A\})(\{\varphi_B\}^T\{\varphi_B\})} \quad (2)$$

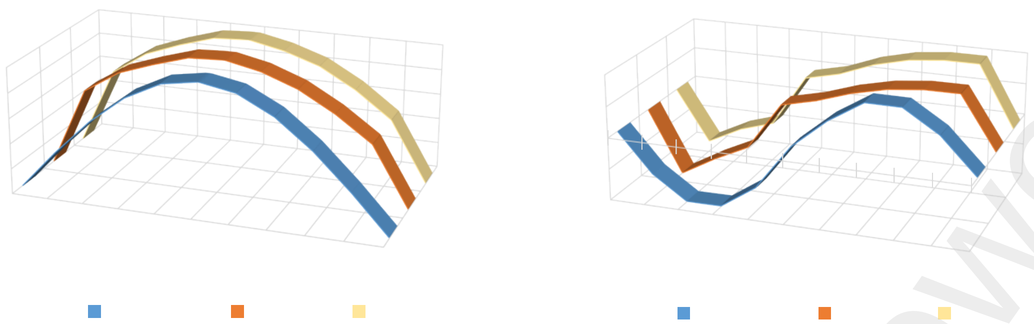

(a) (b)

**Fig. 18.** Mean mode shapes identified from the synthetic data generated in Case 1. (a) Mode 1, 1st bending mode, (b) Mode 2, 2nd bending mode.

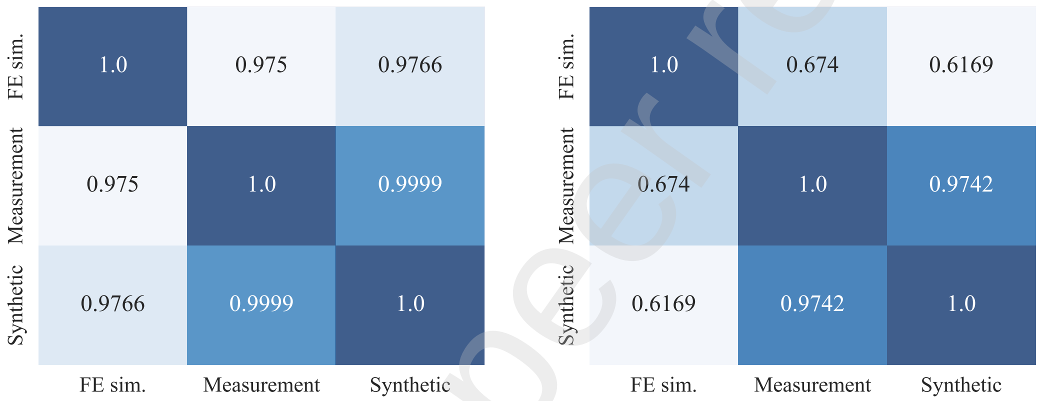


(a) (b)

**Fig. 19.** MAC of mean mode shapes in Case 1. (a) Mode 1, (b) Mode 2

### *4.2. Results of Case 2*

As obtaining sufficient training data is very difficult or even impossible in many actual engineering scenarios, training with a small scale of data has become a natural need for DL modelling. To investigate the performance of the proposed DCCNN under the training scenario with limited data, in this section, only 180 data with impact at Loc. 1 are used for training, other 21 data with impact at Loc. 1 are for validation, and the data with impact at Locs. 5-8 are for testing.

The training histories of losses in Case 2 are shown in Fig. 20. The training loss and validation loss were reduced smoothly and simultaneously. No overfitting appeared in the training procedures. Finally, the losses reached a $10^{-5}$ level, which indicates that the models have learned critical features from the measurement data.

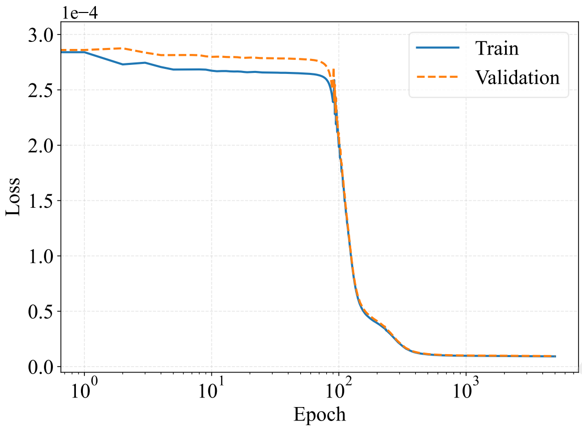


**Fig. 20.** Training history of Case 2

To test the performance of the DCCNN model trained with limited data, the MSE of each test result is visualized in Fig. 21, which calculates the MSE between the measurement data (ground truth) and the synthetic data generated by the DCCNN. The MSE of each individual test data is in a range between 0.004 to 0.028, and the mean MSE of the whole test set is 0.014. Interestingly, comparing the test results of Case 2 to Case 1, the number of training data in Case 2 is only 28.39% of it in Case 1. However, the lower bound, upper bound, and the mean value of the test errors in Case 2 are approximately doubled. The test errors in Case 2 are not greatly affected by the sudden reduction of training data. Fig. 21 also shows a phenomenon that, only using the data with impact at Loc. 1 for training, the MSEs of the synthetic data with impact at Locs. 5-7 are generally in the same range, and the MSEs of the synthetic data with impact at Loc. 8 are apparently lower than those of Locs. 5-7. One possible explanation for this phenomenon is that the DCCNN has only learned the features of the vibration excited by the loads close to the support (Loc. 1). Since Loc.8 is also close to the support, and it is in the symmetric position of Loc. 1, better test results were obtained when the impacts are in Loc. 8 of the test data.

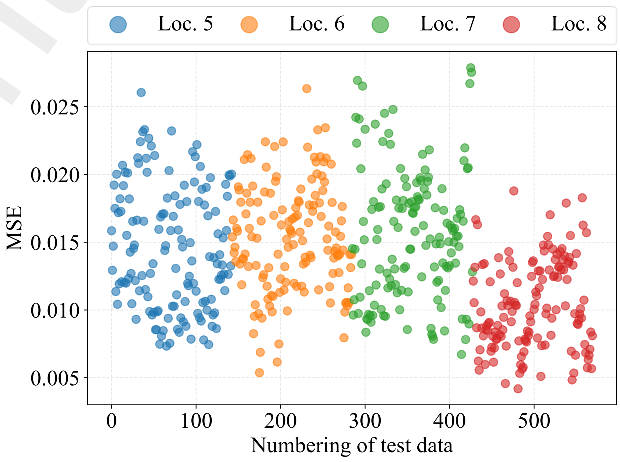


**Fig. 21.** MSE of each test data in Case 2 with the mean value of 0.014

Figs. 22 and 23 demonstrate the two examples of the synthetic data in the test set, which are generated by the proposed DCCNN trained with limited data in Case 2. The two test data are the two used in Figs. 14 and 15. The MSEs of the two test examples are 0.0159 and 0.0081, which are higher and lower than the mean MSE of the whole test set (0.014), respectively. Observing Figs. 22 and 23, when trained with limited data, even though the amplitudes of the synthetic data are not as accurate as those in Figs. 14 and 15 in Case 1, the DCCNN can successfully learn the dominant features of the vibration, like frequencies and phases.

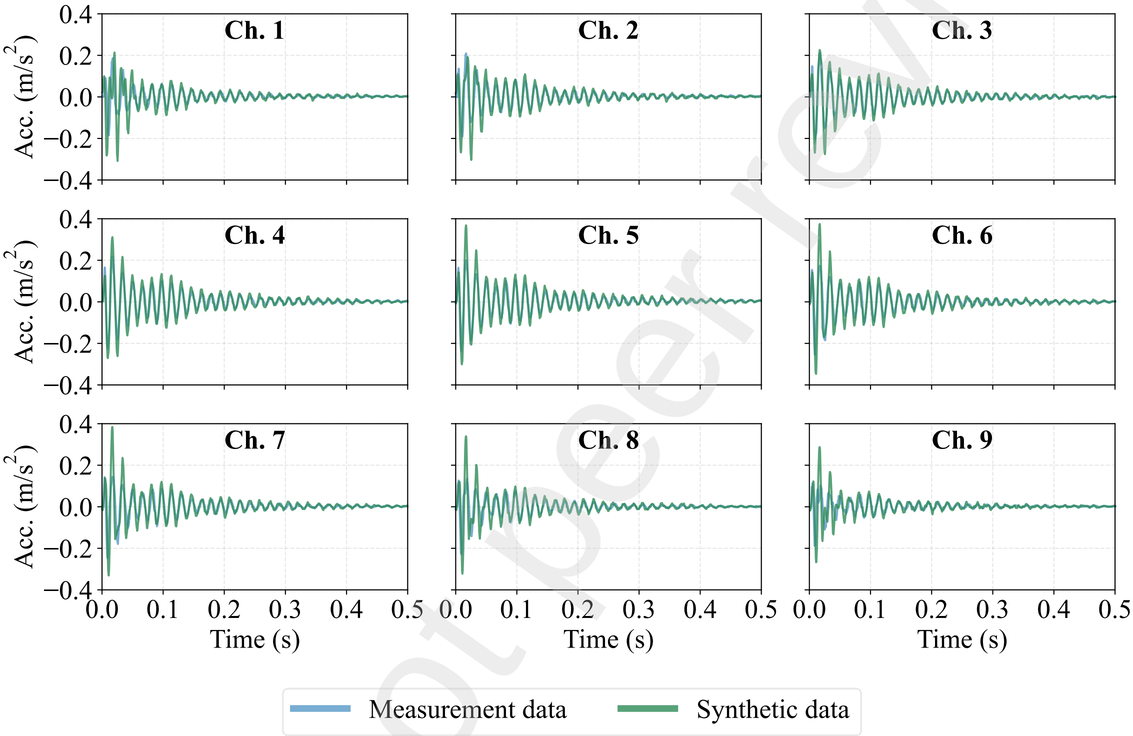


**Fig. 22.** Synthetic data generated by DCCNN (Case 2, impact at Loc. 5, MSE of 0.0159)

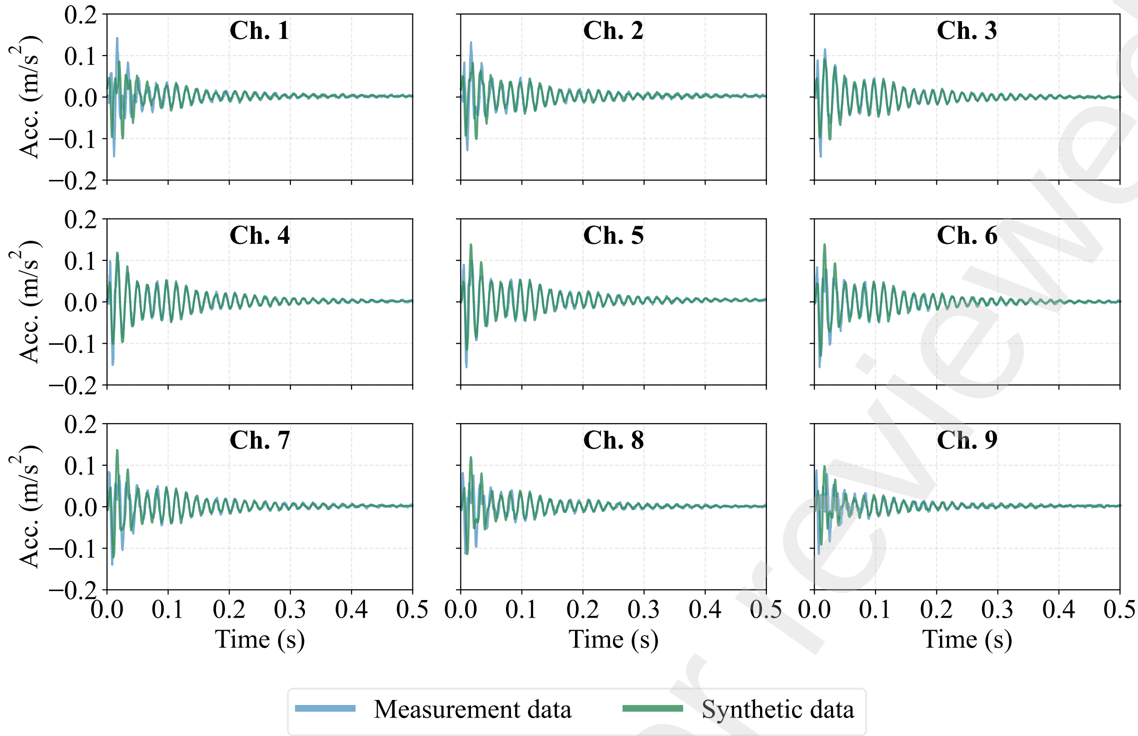


**Fig. 23.** Synthetic data generated by DCCNN (Case 2, impact at Loc.8, MSE of 0.0081)

Then, to investigate the quality of the synthetic data in the frequency domain, we performed FFT on the FE simulation, measurement, and synthetic data. Using Ch. 6 in Fig. 23 as an example, as visualised in Fig. 24, the subplots of waveforms in the first row show the amplitudes of the synthetic data lose some accuracy with the reduction of training data. In the FFT subplots in the second and third rows, the two peaks indicate the synthetic data can successfully reproduce the mode features. In the dB-scale spectrum of synthetic data, the magnitudes over 100 Hz show also lower accuracy than the corresponding measurement data, which proves that DCCNN has the characteristics of low-pass filter, and the components higher than about 100 Hz are depressed.

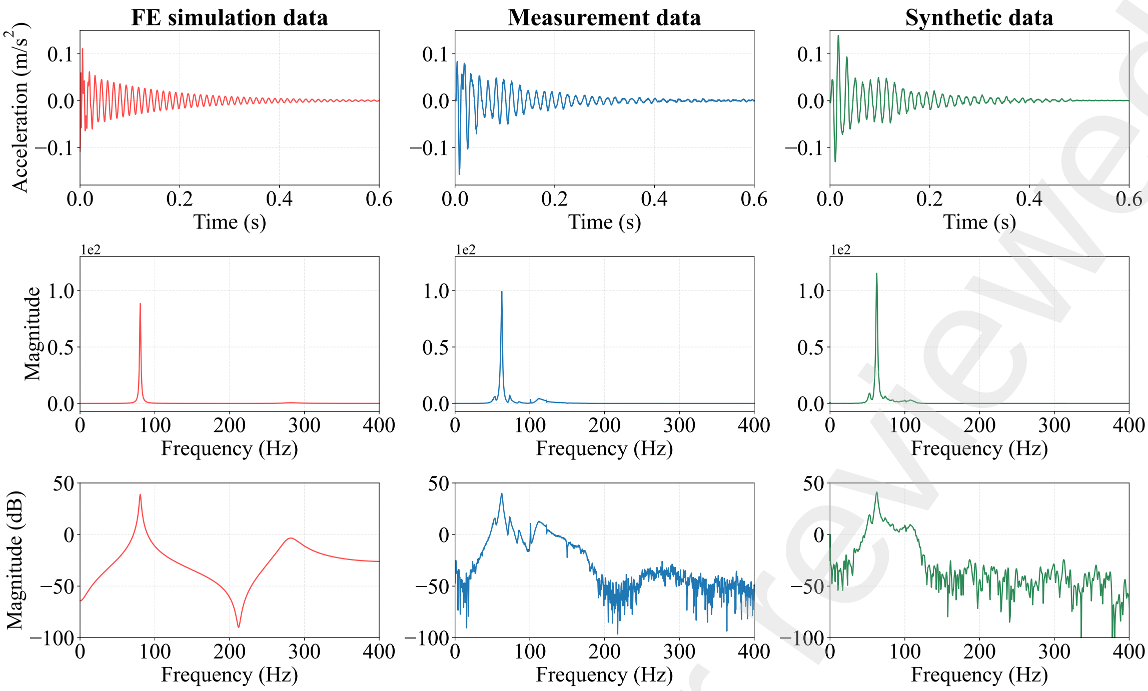


**Fig. 24.** Comparison of FE simulation, measurement, and synthetic data in the frequency domain (impact at Loc. 8, Ch. 6 of the data example in Fig. 23)

Meanwhile, the accuracies of the mean mode shapes identified from the synthetic data in the test set of Case 2 are also analysed. Fig. 25 compares the identified mean mode shapes of the synthetic data in the whole test set to those of the FE simulation and measurement data. Both Modes 1 and 2 can be identified from the synthetic data. The consistencies of the identified mode shapes are shown in Fig. 26. The values of MAC for all the identified mode shapes are higher than 0.98, indicating the accurate representation of the proposed networks even with limited training data.

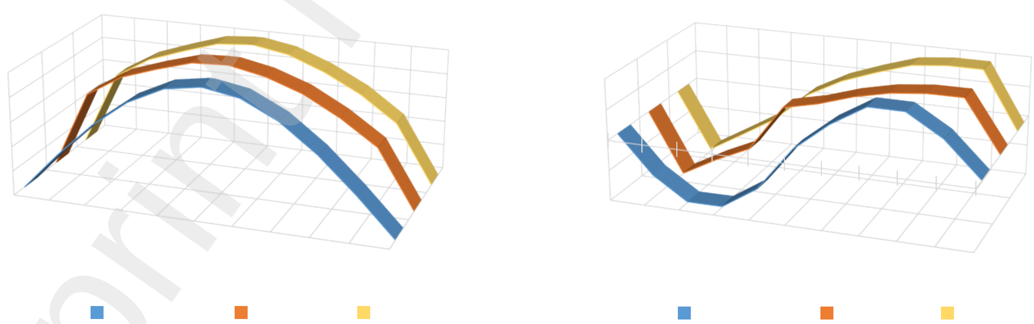

(a) (b)

**Fig. 25.** Mode shapes identified from the synthetic data generated in Case 1. (a) Mode 1: 1$^{st}$ bending mode, (b) Mode 2: 2$^{nd}$ bending mode.

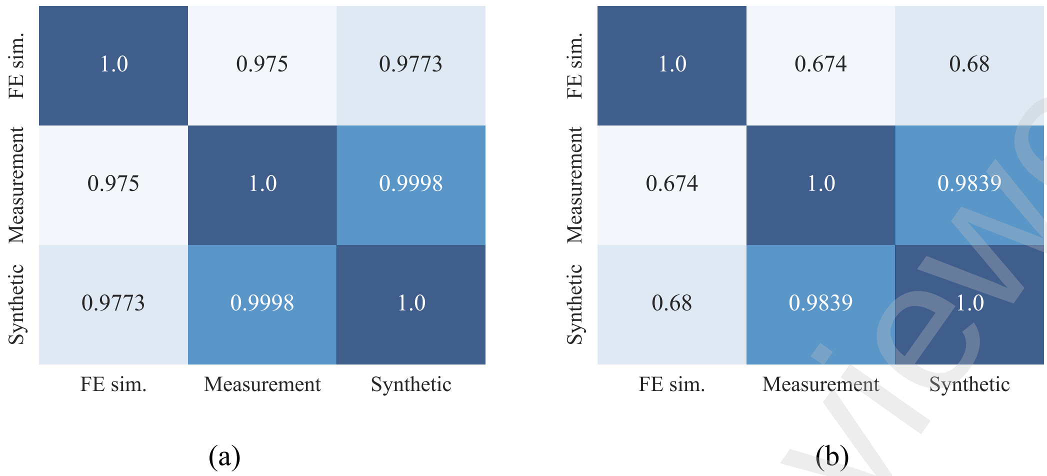


**Fig. 26.** MAC of mode shapes in Case 2. (a) Mode 1, (b) Mode 2

**5. Conclusions**

In this paper, we proposed a novel method to synthesise high-fidelity time-series data. The proposed method consists of experiments, FE simulation, and space projection using DL. Low-fidelity FE simulation data can be transferred to high-fidelity measurement data in an end-to-end manner. A DL model DCCNN was designed for this projecting task. Both physical and numerical vibration experiments were performed to test the proposed method. The remarkable quality of the synthetic data demonstrates the effectiveness of the proposed method. Some detailed conclusions are drawn as follows.

First, the proposed method can accurately synthesise the vibration data excited by the loads that were not used for training and validation. This shows the applicability of the proposed method for synthesising high-fidelity structural dynamics when the desired loads are not available or cannot be applied on real structures.

Second, the proposed method can generate realistic synthetic vibration data of structures without performing FE model updating. Compared to the measurement data acquired directly from the structure, the synthetic vibration data are very accurate when observed in the time domain, frequency domain, natural frequencies, phase, amplitude, and mode shapes. The high-quality synthetic data also indicates the rationality of the design of the DCCNN for the data synthesis task.

Third, the proposed DCCNN has the characteristics of low-pass filter. When in the normal training case with sufficient training data, DCCNN tends to depress the components higher than 200 Hz. When training with limited data, the DCCNN tends to depress the components higher than 100 Hz. Such a feature makes the DL models can be considered with an integrated noise reducer.

The proposed method can contribute to all the downstream tasks, for instance, analyses of structural dynamic behaviours, design optimisation, data-driven identification tasks, etc., which request time-series simulation data. Our future work will be focused on addressing the following limitations. First, the performance of the proposed data synthesis method with other types of loads and structural responses is unknown. Excitations with actuators and forced vibration data will be used to further test and update the proposed method. Second, the DCCNN needs to be slightly refined when the structure and corresponding FE model are changed. Our next work includes the development of a method to model the domain shift and avoid the data required for refining the DCCNN when the structure and FE model are changed. This aims to synthesise dynamic responses of the structure with specified non-existent changes or damage.

## CRediT author statement

**Youqi Zhang:** Conceptualization, Methodology, Software, Formal analysis, Investigation, Validation, Resources, Data Curation, Writing - Original Draft, Visualization, Funding acquisition. **Zhenkun Li:** Software, Formal analysis. **Rui Hao:** Investigation. **Weiwei Lin:** Resources, Funding acquisition. **Lingfang Li:** Software, Formal analysis. **Di Su:** Funding acquisition. All the authors reviewed and edited the manuscript.

## Declaration of competing interest

The authors declare that they have no known competing financial interests or personal relationships that could have appeared to influence the work reported in this paper.

## Acknowledgment

The authors greatly acknowledge the financial support from the Academy of Finland (decision number: 339493). The 2nd and 4th authors are financially supported by the Jane and Aatos Erkko Foundation in Finland. The assistance of the laboratory staff at Aalto University is also gratefully acknowledged.

## References

[1] L. Lombardi, F. De Luca, J. Macdonald, Design of buildings through linear time-history analysis optimising ground motion selection: a case study for RC-MRFs, Engineering Structures, 192 (2019) 279-295.

[2] C. Jin, W.C. Chung, D.-S. Kwon, M. Kim, Optimization of tuned mass damper for seismic control of submerged floating tunnel, Engineering Structures, 241 (2021) 112460.

[3] G. He, D. Cao, Y. Cao, W. Huang, Dynamic modeling and orbit maneuvering response analysis for a three-axis attitude stabilized large scale flexible spacecraft installed with hinged solar arrays, Mechanical Systems and Signal Processing, 162 (2022) 108083.

[4] T.R. Felipe, A.T. Beck, Dynamic analysis of failure paths of truss structures: Benchmark examples including material degradation, Mechanical Systems and Signal Processing, 158 (2021) 107767.

[5] Z. Yang, Y. Li, H. Guan, M. Diao, B.P. Gilbert, H. Sun, L. Xu, Dynamic response and collapse resistance of RC flat plate structures subjected to instantaneous removal of an interior column, Engineering Structures, 264 (2022) 114469.

[6] J. Liu, P. Wang, X. Guo, L. Dai, Y. He, Nonlinear vibration model and response characteristic of drilling risers in deep-sea under soft suspension evacuation condition, Mechanical Systems and Signal Processing, 169 (2022) 108783.

[7] C. Yeung, C.T. Ng, Time-domain spectral finite element method for analysis of torsional guided waves scattering and mode conversion by cracks in pipes, Mechanical Systems and Signal Processing, 128 (2019) 305-317.
[8] L. Li, M. Faisal Haider, H. Mei, V. Giurgiutiu, Y. Xia, Theoretical calculation of circular-crested Lamb wave field in single-and multi-layer isotropic plates using the normal mode expansion method, Structural Health Monitoring, 19 (2020) 357-372.
[9] D. Su, Y. Fujino, T. Nagayama, J.Y. Hernandez, M. Seki, Vibration of reinforced concrete viaducts under high-speed train passage: measurement and prediction including train–viaduct interaction, Structure and Infrastructure Engineering, 6 (2010) 621-633.
[10] Y.z. Lin, Z.h. Nie, H.w. Ma, Structural damage detection with automatic feature-extraction through deep learning, Computer-Aided Civil and Infrastructure Engineering, 32 (2017) 1025-1046.
[11] T. Guo, L. Wu, C. Wang, Z. Xu, Damage detection in a novel deep-learning framework: a robust method for feature extraction, Structural Health Monitoring, 19 (2020) 424-442.
[12] P. Seventekidis, D. Giagopoulos, A. Arailopoulos, O. Markogiannaki, Structural Health Monitoring using deep learning with optimal finite element model generated data, Mechanical Systems and Signal Processing, 145 (2020) 106972.
[13] Y.B. Yang, B. Zhang, Y. Qian, Y. Wu, Contact-Point Response for Modal Identification of Bridges by a Moving Test Vehicle, International Journal of Structural Stability and Dynamics, 18 (2017) 1850073.
[14] D.A. Ramatlo, C.S. Long, P.W. Loveday, D.N. Wilke, Physics-based modelling and simulation of reverberating reflections in ultrasonic guided wave inspections applied to welded rail tracks, Journal of Sound and Vibration, 530 (2022) 116914.
[15] C. Boller, Chang, F. K., & Fujino, Y. (Eds.). , Encyclopedia of structural health monitoring, Wiley Online Library, 2009.
[16] L. Sun, Z. Shang, Y. Xia, S. Bhowmick, S. Nagarajaiah, Review of bridge structural health monitoring aided by big data and artificial intelligence: From condition assessment to damage detection, Journal of Structural Engineering, 146 (2020) 04020073.
[17] T. Khuc, T.A. Nguyen, H. Dao, F.N. Catbas, Swaying displacement measurement for structural monitoring using computer vision and an unmanned aerial vehicle, Measurement, 159 (2020) 107769.
[18] M. Sanayei, A. Khaloo, M. Gul, F.N. Catbas, Automated finite element model updating of a scale bridge model using measured static and modal test data, Engineering Structures, 102 (2015) 66-79.
[19] A. Öchsner, M. Merkel, One-Dimensional Finite Elements, Springer, 2013.
[20] J.N. Reddy, Introduction to the finite element method, McGraw-Hill Education, 2019.
[21] F. Hartmann, C. Katz, Structural analysis with finite elements, Springer Science & Business Media, 2004.
[22] H. Salehi, R. Burgueño, Emerging artificial intelligence methods in structural engineering, Engineering structures, 171 (2018) 170-189.
[23] R.B. Corotis, An overview of uncertainty concepts related to mechanical and civil engineering, ASCE-ASME Journal of Risk and Uncertainty in Engineering Systems Part B: Mechanical Engineering, 1 (2015) 040801.
[24] Y. Bao, Z. Tang, H. Li, Y. Zhang, Computer vision and deep learning–based data anomaly detection method for structural health monitoring, Structural Health Monitoring, 18 (2019) 401-421.
[25] Y. Zhang, Z. Tang, R. Yang, Data anomaly detection for structural health monitoring by multi-view representation based on local binary patterns, Measurement, 202 (2022) 111804.
[26] E. Simoen, G. De Roeck, G. Lombaert, Dealing with uncertainty in model updating for damage assessment: A review, Mechanical Systems and Signal Processing, 56 (2015) 123-149.
[27] M. Machado, S. Adhikari, J. Dos Santos, J. Arruda, Estimation of beam material random field properties via sensitivity-based model updating using experimental frequency response functions, Mechanical Systems and Signal Processing, 102 (2018) 180-197.

[28] S. Sehgal, H. Kumar, Structural dynamic model updating techniques: a state of the art review, Archives of Computational Methods in Engineering, 23 (2016) 515-533.
[29] H.-P. Chen, T.S. Maung, Regularised finite element model updating using measured incomplete modal data, Journal of Sound and Vibration, 333 (2014) 5566-5582.
[30] A. Mojtahedi, H. Hokmabady, A. Yaghubzadeh, S. Mohammadyzadeh, An improved model reduction-modal based method for model updating and health monitoring of an offshore jacket-type platform, Ocean Engineering, 209 (2020) 107495.
[31] W. Zhao, L. Yang, C. Dang, R. Rocchetta, M. Valdebenito, D. Moens, Enriching stochastic model updating metrics: An efficient Bayesian approach using Bray-Curtis distance and an adaptive binning algorithm, Mechanical Systems and Signal Processing, 171 (2022) 108889.
[32] B. Goller, G. Schueller, Investigation of model uncertainties in Bayesian structural model updating, Journal of sound and vibration, 330 (2011) 6122-6136.
[33] J. Jang, A. Smyth, Bayesian model updating of a full-scale finite element model with sensitivity-based clustering, Structural Control and Health Monitoring, 24 (2017) e2004.
[34] A. Esfandiari, An innovative sensitivity-based method for structural model updating using incomplete modal data, Structural Control and Health Monitoring, 24 (2017) e1905.
[35] M. Rezaiee-Pajand, A. Entezami, H. Sarmadi, A sensitivity-based finite element model updating based on unconstrained optimization problem and regularized solution methods, Structural Control and Health Monitoring, 27 (2020) e2481.
[36] S. Cong, S.-L.J. Hu, H.-J. Li, FRF-based pole-zero method for finite element model updating, Mechanical Systems and Signal Processing, 177 (2022) 109206.
[37] M.H. Jalali, D.G. Rideout, Frequency-based decoupling and finite element model updating in vibration of cable–beam systems, Journal of Vibration and Control, 28 (2022) 1520-1535.
[38] T. Marwala, Finite-element-model updating using computional intelligence techniques: Applications to structural dynamics, Springer, 2010.
[39] P. Noever-Castelos, D. Melcher, C. Balzani, Model updating of a wind turbine blade finite element Timoshenko beam model with invertible neural networks, Wind Energy Science, 7 (2022) 623-645.
[40] J. Jung, H. Jun, P.-S. Lee, Self-updated four-node finite element using deep learning, Computational Mechanics, 69 (2022) 23-44.
[41] J. Naranjo-Pérez, M. Infantes, J.F. Jiménez-Alonso, A. Sáez, A collaborative machine learning-optimization algorithm to improve the finite element model updating of civil engineering structures, Engineering Structures, 225 (2020) 111327.
[42] I. Goodfellow, Y. Bengio, A. Courville, Deep learning, MIT press, 2016.
[43] Y. LeCun, Y. Bengio, G. Hinton, Deep learning, nature, 521 (2015) 436-444.
[44] X. Ye, T. Jin, C. Yun, A review on deep learning-based structural health monitoring of civil infrastructures, Smart Struct. Syst, 24 (2019) 567-585.
[45] Y. Bao, Z. Chen, S. Wei, Y. Xu, Z. Tang, H. Li, The state of the art of data science and engineering in structural health monitoring, Engineering, 5 (2019) 234-242.
[46] R. Zhao, R. Yan, Z. Chen, K. Mao, P. Wang, R.X. Gao, Deep learning and its applications to machine health monitoring, Mechanical Systems and Signal Processing, 115 (2019) 213-237.
[47] Y.J. Cha, W. Choi, O. Büyüköztürk, Deep learning-based crack damage detection using convolutional neural networks, Computer-Aided Civil and Infrastructure Engineering, 32 (2017) 361-378.
[48] Y.J. Cha, W. Choi, G. Suh, S. Mahmoudkhani, O. Büyüköztürk, Autonomous structural visual inspection using region-based deep learning for detecting multiple damage types, Computer-Aided Civil and Infrastructure Engineering, 33 (2018) 731-747.
[49] C.-Z. Dong, F.N. Catbas, A review of computer vision–based structural health monitoring at local and global levels, Structural Health Monitoring, 20 (2021) 692-743.
[50] O. Abdeljaber, O. Avci, M.S. Kiranyaz, B. Boashash, H. Sodano, D.J. Inman, 1-D CNNs for structural damage detection: Verification on a structural health monitoring benchmark data, Neurocomputing, 275 (2018) 1308-1317.
[51] Y. Zhang, Y. Miyamori, S. Mikami, T. Saito, Vibration-based structural state identification by a 1-dimensional convolutional neural network, Computer-Aided Civil and Infrastructure Engineering, 34 (2019) 822-839.

[52] O. Abdeljaber, O. Avci, S. Kiranyaz, M. Gabbouj, D.J. Inman, Real-time vibration-based structural damage detection using one-dimensional convolutional neural networks, Journal of Sound and Vibration, 388 (2017) 154-170.
[53] X. Hou, Y. Zeng, J. Xue, Detecting structural components of building engineering based on deep-learning method, Journal of Construction Engineering and Management, 146 (2020) 04019097.
[54] Y. Zhang, Z. Li, R. Hao, W. Lin, L. Li, D. Su, Vibration Data Synthesis by using Finite Element Analysis and Artificial Neural Network, 8th World Conference on Structural Control and Monitoring (8WCSCM), IASCM Orlando, Florida, USA, 2022.
[55] Y. LeCun, A theoretical framework for back-propagation, Proceedings of the 1988 connectionist models summer school, 1988, pp. 21-28.
[56] A. Van Den Oord, S. Dieleman, H. Zen, K. Simonyan, O. Vinyals, A. Graves, N. Kalchbrenner, A.W. Senior, K. Kavukcuoglu, WaveNet: A generative model for raw audio, SSW, 125 (2016) 2.
[57] D. Rethage, J. Pons, X. Serra, A wavenet for speech denoising, 2018 IEEE International Conference on Acoustics, Speech and Signal Processing (ICASSP), IEEE, 2018, pp. 5069-5073.
[58] A. Oord, Y. Li, I. Babuschkin, K. Simonyan, O. Vinyals, K. Kavukcuoglu, G. Driessche, E. Lockhart, L. Cobo, F. Stimberg, Parallel wavenet: Fast high-fidelity speech synthesis, International conference on machine learning, PMLR, 2018, pp. 3918-3926.
[59] Y. Lu, P. Xiang, P.-s. Dong, X. Zhang, J. Zeng, Analysis of the effects of vibration modes on fatigue damage in high-speed train bogie frames, Engineering Failure Analysis, 89 (2018) 222-241.
[60] X.-R. Huang, L. Jézéquel, S. Besset, L. Li, O. Sauvage, Nonlinear hybrid modal synthesis based on branch modes for dynamic analysis of assembled structure, Mechanical Systems and Signal Processing, 99 (2018) 624-646.
[61] D.P. Kingma, J. Ba, Adam: A method for stochastic optimization, arXiv preprint arXiv:1412.6980, (2014).

# High-Fidelity Time-Series Data Synthesis based on Finite Element Simulation and Data Space Projection

Youqi Zhang[a, *], Zhenkun Li[a], Rui Hao[a], Weiwei Lin[a], Lingfang Li[b], and Di Su[c]

[a] *Department of Civil Engineering, School of Engineering, Aalto University, Espoo, Finland*

[b] *Department of Civil and Environmental Engineering, The Hong Kong Polytechnic University, Hong Kong, China*

[c] *Department of Civil Engineering, The University of Tokyo, Tokyo, Japan*

[*] Corresponding author: Email: youqi.zhang@aalto.fi

**Abstract:** Dynamic responses can provide rich information for supporting the entire life cycle of structures, and they can either be measured from actual structures or simulated using the finite element (FE) method. For the FE simulation, insufficient fidelity of simulation data can significantly affect the confidence of analysis results, while FE model updating methods can partially address this problem by reducing the simulation error. However, most FE model updating methods inevitably update the hyperparameters of FE models using sophisticated algorithms with high computational complexities. Thus, one question was raised: whether there is a projection that can transfer the FE simulation data to the corresponding measurement data directly without performing FE model updating? To achieve this, we proposed a data synthesis method using FE simulation and deep learning space projection, which can be used to synthesize high-fidelity dynamic responses excited by some unseen load patterns in the measurement. A Dilated Causal Convolutional Neural Network (DCCNN) was designed for realising the space projection. Vibration experiments were conducted on both an I-shaped steel beam and the corresponding FE model to establish datasets and test the proposed method. The quality of the synthetic data was analysed in both the time domain and the frequency domain. The accurate amplitudes, natural frequencies, and mode shapes of the synthetic data successfully demonstrate the effectiveness of the proposed high-fidelity data synthesis method.

**Keywords:** data synthesis, finite element analysis, space projection, Dilated Causal Convolutional Neural Network

## 1. Introduction

Measurement data of dynamic behaviours is fundamental for supporting the entire life cycle of structures, which includes design optimization [1, 2], analysis of structural behaviours [3-9], health assessment, damage prognostics [10-12], development of analytical methods [13, 14], etc. Powered by advanced sensing technology and structural health monitoring (SHM) systems [15], dynamic structure behaviours can be observed, and the corresponding measurement data can be acquired. However, in many engineering scenarios, it is challenging or even impossible to acquire measurement data from structures [16, 17]. To address this challenge, finite element (FE) models are widely used for simulating structural dynamics and analysing structural performance. One crucial factor that affects the results of analyses is the quality or fidelity of simulation data. Indeed, deviations between the FE simulation data and the measured dynamic responses of real structures are inevitable [18], and the insufficient fidelity of simulation data can greatly affect the confidence of analysis results.

The reasons for the deviations between FE simulation and measurement data mainly consist of three perspectives. Firstly, FE simulation is based on many assumptions and approximations [19-21], for instance, constant axial stiffness *EA* and the transition from continuum to discrete. It is impossible to consider all the properties of structures and model them accurately, resulting in inevitable modelling deviations. Secondly, measurements of actual structures involve enormous uncertainties and random processes [22, 23], such as boundary conditions and noise, which are difficult to be modelled accurately. Thirdly, as sensor systems are not perfect, measurement error appears in all the observation data [24, 25], which also increases the difference between FE simulation data and measurement data. Consequently, time-series data generated by FE simulation and measurement data are not in the identical data space.

FE model updating methods [26-28] can partially address the problem as aforementioned. FE model updating methods aim to minimize the deviation between FE models and actual structures. Typical FE model updating methods include mode-based updating methods [18, 29, 30], Bayesian methods [31-33], sensitivity-based updating methods [34, 35], frequency-based updating methods [36, 37], and machine learning-based methods [38-41], etc. Most of the existing FE model updating methods align the dominant frequency features or modal features of the FE models with the actual structures. However, most model updating methods inevitably update the hyperparameters of FE models using sophisticated algorithms with high computational complexities, and it is still challenging to simulate "high-fidelity" complex dynamic responses even using the updated FE models. One example is the simulation of structural dynamics using FE analysis. Comparing the FE simulation data of vibration to the measurement data in a short period or in the dB-scale frequency domain, apparent differences tend to be observed. Although the FE model updating methods can align the natural frequencies of the FE models to the actual structures, damping modelling can also greatly influence the fidelity of simulation data. Because of the high complexity of damping mechanism, it is challenging to model damping accurately in real engineering scenarios. Rayleigh damping, as one of the most widely adopted damping modelling methods, combines mass-proportional damping and stiffness-proportional damping. However, it does not consider the energy dissipation of friction in supports, sound emission, anchor losses, or even thermoelastic damping, resulting in some possible loss of fidelity in the simulation of structural dynamics. Therefore, simulation data generated by numerical methods are prone to be in different data space from that of measurement data. Hence, there is a need to further minimize the deviation between the data spaces of FE simulation and measurement data for improving the quality of the FE simulation data. This problem can be considered as a space projection task, which targets to project the data from the simulation data space to the measurement data space. Such data space projection can be achieved using modelling methods like Deep Learning (DL) [42] in an end-to-end manner.

DL has made a great wave of data-driven methods since 2015 [43], and it is becoming increasingly prevalent in the engineering field. Different from the traditional knowledge-based modelling approaches, DL is a data-driven method which can be applied with zero domain knowledge. Correlations between two datasets can be built automatically or projections between two different data spaces can be established automatically by training DL models. Countless examples of DL applications demonstrate DL's power in solving real-world engineering problems, for instance, SHM [16, 44-46], especially image-based structural damage detection [47-49] and vibration-based structural state identification [50-52], detection of structural components [53], etc. Meanwhile, DL has also been used for style transfer tasks in the image processing and audio processing fields. Therefore, DL has demonstrated its merits for data transfer tasks or modelling complex projection between two datasets, and has shown a full potential to achieve the projection from the simulation data space to the measurement data space.

In this article, we proposed a method to generate high-fidelity time-series synthetic data. Projections from the FE simulation data space to the measurement data space are built using DL. To the best of our knowledge, this is the first attempt to synthesize time-series data using FE simulation and DL space projection. The projection enables a significant quality improvement of the time-series simulation data without performing FE model updating. One suitable application scenario for the proposed method is that, when dynamic responses of structures excited by some unseen load patterns are not available in the real world, the proposed method can achieve high-fidelity synthetic data in an end-to-end manner. Moreover, the high-fidelity time-series synthetic data generated by the proposed method can benefit all the downstream tasks as mentioned in the first paragraph. As a reminder, this article is organized into 5 sections. After introducing the background in Section 1, the proposed data synthesis method is presented in Section 2. Then Section 3 describes the experiments and datasets, and Section 4 discusses the results. Finally, some conclusions are drawn in Section 5. This idea was initialized in a short conference paper [54], in which we briefly proved the concept using a fully-connected neural network. In this manuscript, we proposed a new light-weighted DL model with much fewer trainable parameters, tested the performance of the method more rationally, investigated the case with both sufficient and limited training data, performed quantitative analyses in both time and frequency domains, and evaluated the quality of synthetic data with modal analyses.

## 2. Methodology

### *2.1. Workflow of the proposed method*

The proposed method for time-series data synthesis is illustrated in Fig. 1. It consists of physical experiment, FE simulation, and data space projection. Identical external loads are attempted to be applied on both the actual specimen and the FE model. Even though the measurement errors of load amplitudes and manual errors of impact locations are inevitable, the errors of impact forces and locations can be managed in limited ranges. These errors are considered in the process of the proposed method which can provide some robustness to the space projection model. To prove the concept of the proposed method, vibration experiments with only hammer impact loads were performed on both a physical specimen and the corresponding numerical model. Actuators can also be used to apply excitations on structures because they can apply the assigned loads on the structures with other load patterns.

The dynamic behaviour of the physical specimen is measured using an acceleration sensor system, and the corresponding dynamic behaviour of the numerical model is simulated using FE analysis. Then a paired dataset of measurement data and FE simulation data can be obtained which are used for training, validating, and testing the DL models. Finally, a projection from the data space of the FE simulation to the data space of the measurement data is established by DL modelling. The FE simulation dataset is used as input for the DL model, and the measurement dataset is for the ground truth. Consequently, the synthetic data can be predicted by the DL model.

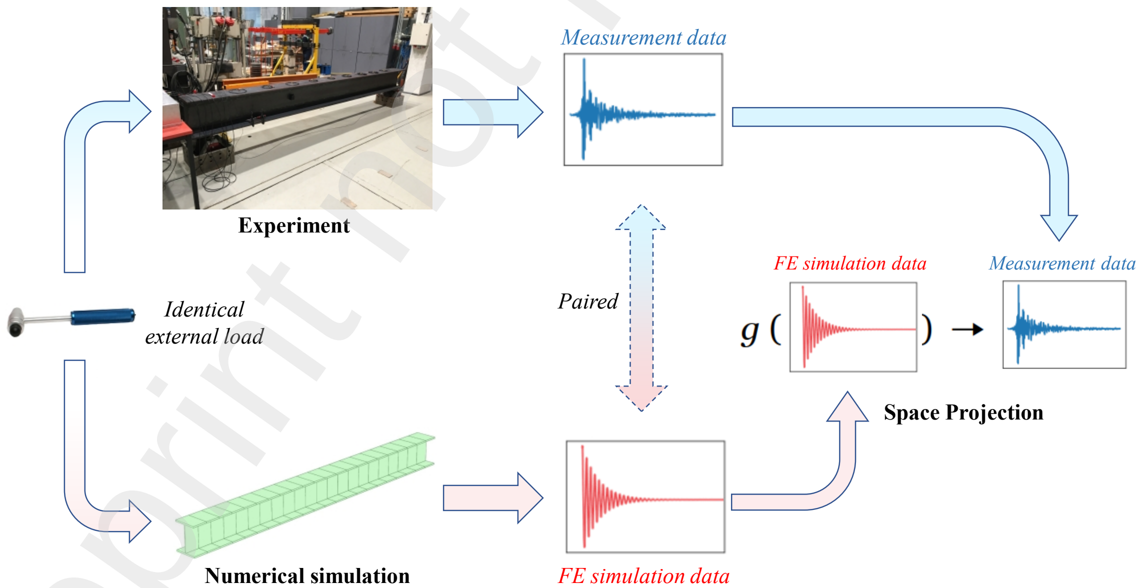


**Fig. 1.** Architecture of the proposed method for time-series data synthesis

### *2.2. DL modelling*

DL is a prevalent data-driven modelling method. It can approximate correlations between two datasets through a training procedure, with no requirement for domain knowledge. After designing the architecture of the DL model according to the specific tasks, the training process can be realised in three steps. Firstly, training data are fed into the DL model, and then corresponding predictions are obtained. Secondly, modelling loss is calculated by comparing the predictions and the ground truth via a certain loss function, e.g., mean square error (MSE). Finally, the loss is minimised using back-propagation [55] and gradient descent.

The task of DL in the proposed method is to transfer the vibration data from the simulation space to the measurement space as illustrated in Fig. 1. As this is a time-series data processing, we designed a Dilated Causal Convolutional Neural Network (DCCNN), which stacks multiple Dilated Causal Convolution (DCC) layers as its core components.

DCC is a specific type of convolution. Compared to the ordinary 1-D convolution, DCC has the operation of dilation and causal constraint. Dilation describes how convolutional kernels slide on the input data. The kernels are applied on an area that is larger than the kernel size by skipping input values with a certain step. The skipped step is called dilation rate. Stacking a few Dilated Convolution layers can effectively expand the receptive field. Causal constraint makes the prediction not depend on any neuron in the future timesteps. Such a feature makes it feasible for real-time processing, which provides a great potential of DCCNNs for being integrated into SHM systems or digital twin systems in the future. Fig. 2 shows an example of a DCCNN which includes 3 DCC layers with dilation rates of 1, 2, and 4. The receptive field reaches 16 for each neuron in the output layer in the illustration. Based on the unique characteristics of DCC, it is widely used for processing temporal data, e.g., audio generation [56], speech denoising [57], speech synthesis [58], etc. Since audio signal is a specific type of vibration data collected by microphones, it shares high similarities with the vibration data acquired from structures. Therefore, a DCCNN is proposed for time-series data synthesis.

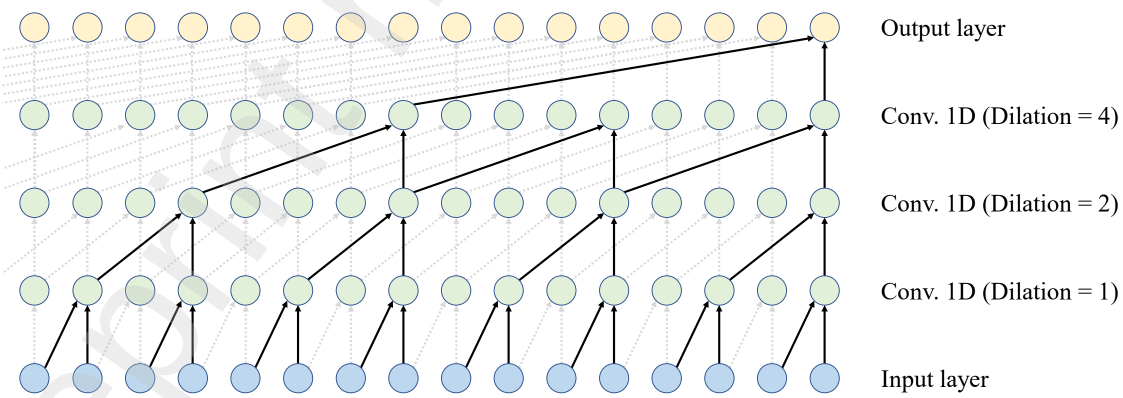


**Fig. 2.** Example of a DCCNN

The structure of the proposed DCCNN is shown in Fig. 3. In total 8 DCC layers and 8 Leaky Rectified Linear Unit (ReLU) layers are designed between the input layer and the output layer. The dilation rates are $2^i$ ($i = 0,\cdots,7$) in the DCC layers. The number of kernels is 32 and the kernel length is 5. As a result, the receptive field for each value in the prediction is 512, which is 12.8% (512/4000) of the total data length. The number of DCC layers was determined by balancing the receptive field and the number of trainable parameters with several rounds of trial and error. Insufficient receptive fields tend to cause very low amplitudes in the latter part of the synthetic data. Long receptive fields request deep network architecture with more trainable parameters, which is computationally costly. Leaky ReLU activation function, as explained in Fig. 4, is designed after each DCC layer to induce nonlinearity in the representation of the network, where $\alpha$ of 0.5 is used to represent the negative slope.

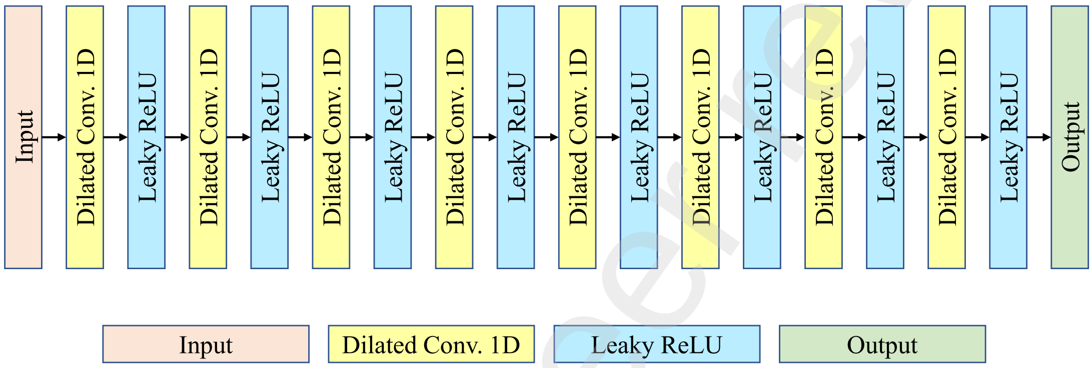


**Fig. 3.** Structure of the proposed DCCNN

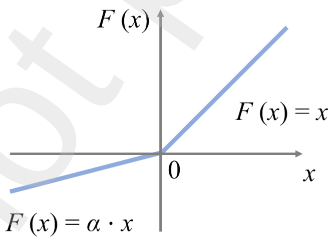


**Fig. 4.** Illustration of Leaky ReLU

Detailed parameters of the DCCNN are summarized in Table 1. The total number of trainable parameters is only 37,833, which is very close to the number of samples in each datum 36,000 (4000 samples × 9 channels). Designing similar numbers of trainable parameters in the DCCNN as the number of data samples aims to prevent over-fitting.

**Table 1.** Parameters of the DCCNN

| Layer | Output shape | Parameter | Number of Parameters |
|---|---|---|---|
| Input | 4000×9 | - | 0 |
| Conv1D_1 | 4000×32 | Dilation rate = 1 | 1472 |
| Leaky ReLU | 4000×32 | $\alpha = 0.5$ | 0 |
| Conv1D_2 | 4000×32 | Dilation rate = 2 | 5152 |
| Leaky ReLU | 4000×32 | $\alpha = 0.5$ | 0 |
| Conv1D_3 | 4000×32 | Dilation rate = 4 | 5152 |
| Leaky ReLU | 4000×32 | $\alpha = 0.5$ | 0 |
| Conv1D_4 | 4000×32 | Dilation rate = 8 | 5152 |
| Leaky ReLU | 4000×32 | $\alpha = 0.5$ | 0 |
| Conv1D_5 | 4000×32 | Dilation rate = 16 | 5152 |
| Leaky ReLU | 4000×32 | $\alpha = 0.5$ | 0 |
| Conv1D_6 | 4000×32 | Dilation rate = 32 | 5152 |
| Leaky ReLU | 4000×32 | $\alpha = 0.5$ | 0 |
| Conv1D_7 | 4000×32 | Dilation rate = 64 | 5152 |
| Leaky ReLU | 4000×32 | $\alpha = 0.5$ | 0 |
| Conv1D_8 | 4000×32 | Dilation rate = 128 | 5152 |
| Leaky ReLU | 4000×32 | $\alpha = 0.5$ | 0 |
| Output | 4000×9 | | 297 |
| ***In total*** | - | | ***37,833*** |

## 3. Experiment

As vibration data is one of the representative types of time-series data, we designed an experiment which uses vibration data to validate the proposed time-series data synthetic method. As introduced in Section 2, the proposed method comprises three main parts: physical experiment, FE simulation, and space projection. The details of those three parts in the case studies are introduced in the following subsections, respectively.

### *3.1. Physical experiment*

Figs. 5 and 6 show the layout of the physical experiment for establishing the measurement dataset of vibration data. An I-shaped steel beam was selected as the specimen owing to its moderate complexity as a real structure. The total length of the beam is 4.4 m, and the span length is 4.0 m. The beam was simply supported at its two ends, and the imperfect boundary conditions increased the uncertainties in the vibration data.

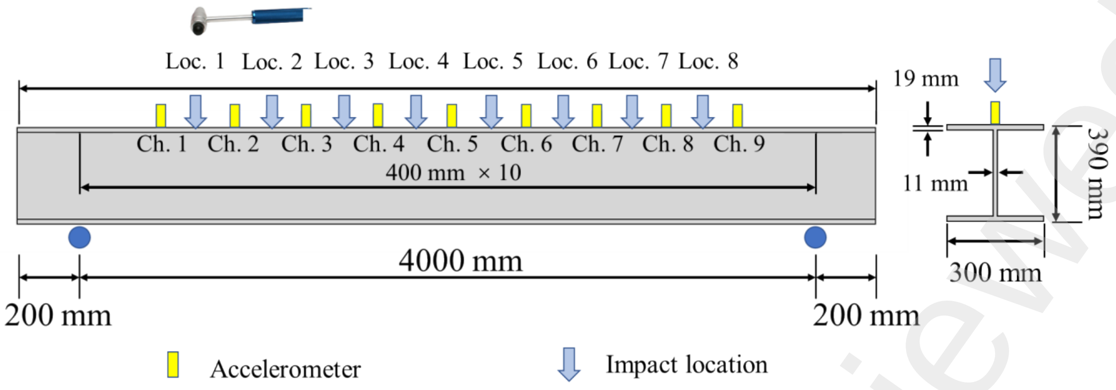


**Fig. 5.** Locations of accelerometers and hammer impacts

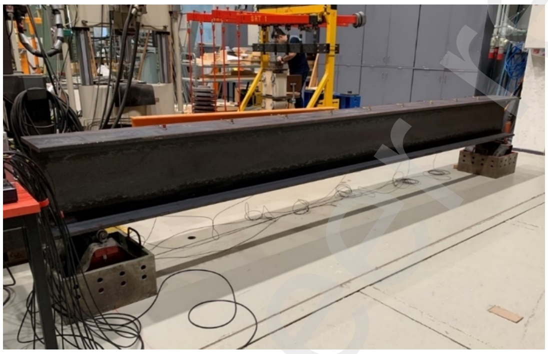

**Fig. 6.** Specimen of the vibration experiment

The vibration measurement system consists of Brüel & Kjær 4371 accelerometers, Brüel & Kjær 2635 amplifiers, an electric hammer, a Measurement Computing DT9834 multifunction USB data acquisition (DAQ) device, and a laptop computer. In total 9 accelerometers were evenly distributed on the upper flange of the beam, named from Ch. 1 to Ch. 9. The sampling frequency is 2000 Hz, and the measurement time after each hammering is 2.0 s. Thus, the vibration data of each measurement has a shape of 4000 samples × 9 channels. The measurement time of 2.0 s was determined according to the time for a free-damped vibration of the structure to vanish. Observing the variation of amplitudes of the free-damped vibration of the beam, it takes about 1.0 s from starting to the approximate end. Thus, doubling the time length of free damped vibration, 2.0 s was used to ensure sufficient information to be included in the measurement data. An electric hammer was used to measure the impact force, which triggers the measurement of free-damped vibration.

The impact locations are in the midpoint of every two adjacent accelerometers. In total, the hammer impact loads were applied on 8 locations, termed from Loc. 1 to Loc. 8. The impact forces are random and generally lower than 10 N. Examples of a hammer impact force and the corresponding response of the beam are shown in Fig. 7. The impact location is Loc. 1, and the vibration measured in Ch. 6 is shown in Fig. 7b. Because the I-beam is modelled as a structure with multiple degrees of freedom, the vibration of the beam can be considered as the superposition of multiple vibration modes. Additionally, the imperfect boundary conditions on the supports also increase the complexity of the vibration. Therefore, Fig. 7b does not show a curve with monotonically decreasing amplitudes. The numbers of hammerings in all locations are summarized in Table 2. Over 140 times of impact were applied at each location. In total, 1277 free-damped vibration data were acquired. The measurement data also contain the noise components caused by the laboratory environment, for instance, the noise of load test, electric saw cutting, moving and dropping of heavy materials, etc. Raw measurement data was used directly without any noise reduction or pre-processing.

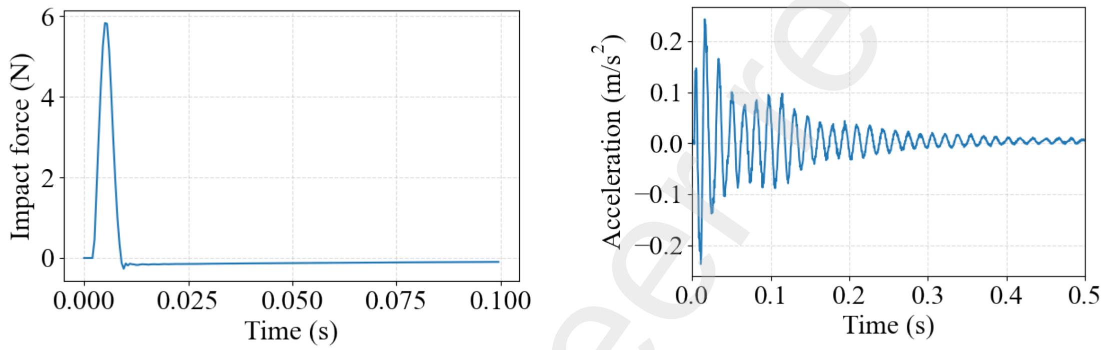


(a) (b)

**Fig. 7.** Examples of hammer impact load and measured vibration. (a) impact load at Loc. 1, (b) measurement data of beam vibration (Ch. 6)

**Table 2.** Data distribution

| Impact location | 1 | 2 | 3 | 4 | 5 | 6 | 7 | 8 | In total |
|---|---|---|---|---|---|---|---|---|---|
| Number of data | 201 | 218 | 145 | 143 | 142 | 143 | 142 | 143 | 1,277 |

### *3.2. FE simulation*

To build the simulation dataset and test the proposed data synthesis method, a FE model of the steel beam was established using ABAQUS, as shown in Fig. 8. We intentionally created a FE model with high modelling error or misspecification in the following ways to check whether the proposed method can yield a satisfactory result even with inaccurate modelling. First, the FE model consists of only 22 beam elements (B31) and 23 nodes. The length of each element is 0.20 m. The beam is simply supported with a span length of 4.0 m. The FE model with limited details is prone to inaccurate solutions. Second, no model updating or calibration was performed on the FE model. The model parameters, such as Young's modulus of 210 GPa, Poisson ratio of 0.3, density of 7850 kg/m$^3$, and boundary conditions of a simply-supported beam, were not calibrated to match the experimental results. Third, the Rayleigh damping factors $\alpha$ and $\beta$ in the FE model were empirically assigned $\alpha$

of $2\times10^{-3}$ and $\beta$ of $5\times10^{-5}$, respectively Those two parameters were not aligned with the damping ratios of the physical specimen calculated from the measurement data. Overall, the deviations between the physical specimen and the FE model were created deliberately with high misspecification for testing purposes.

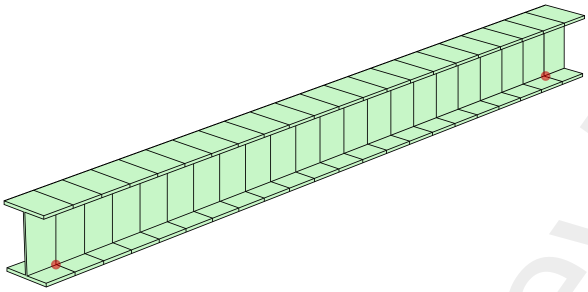

**Fig. 8.** Finite element model of the beam

The method for modelling the structural dynamics of the beam was mode superposition , which superimposes the weighted displacement of each mode shape, as shown in the examples [59, 60]. This experiment considered the superposition of the first 30 modes, which include vertical modes, horizontal modes, and longitudinal modes. As only vertical vibration is measured and discussed, only the vertical modes involved in the mode superposition are shown in Fig. 9, which are the first 4 orders of bending modes.

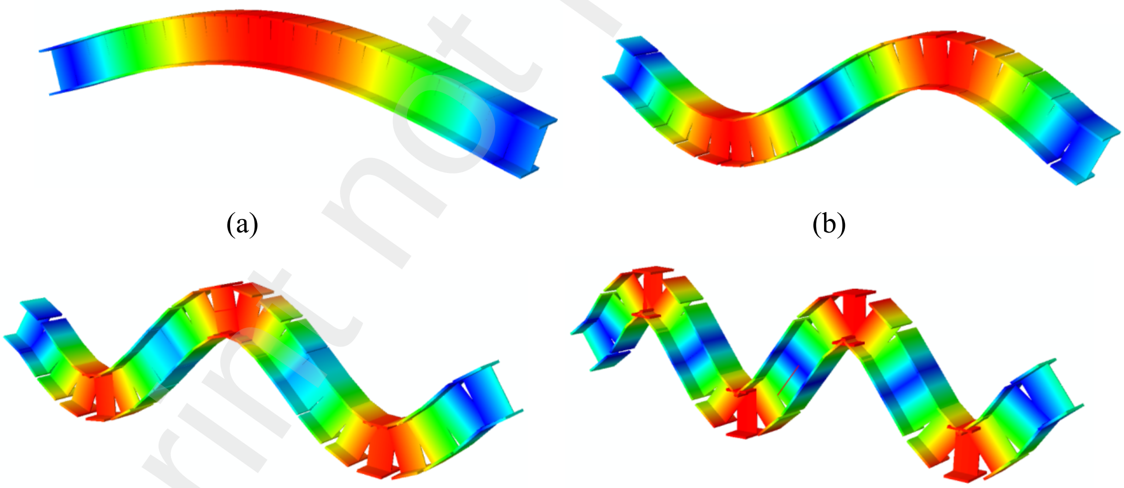

(a) (b)

(c) (d)

**Fig. 9.** Vertical bending modes of the FE model with natural frequencies of 80.49 Hz, 280.08 Hz, 534.13 Hz, and 840.93 Hz

The impact loads recorded in the vibration experiment were applied to the corresponding locations of the FE model. As a result, 1277 simulation data were obtained as the pairs of the corresponding measurement data. Fig. 10 shows an example of the simulation data (vibration at Ch.

6, hammer impact at Loc. 1 with the load shown in Fig. 7a). Different from its corresponding measurement data shown in Fig. 7b, the simulation data have a higher frequency, and the amplitudes of the simulation data decrease monotonically according to the prescribed Rayleigh damping.

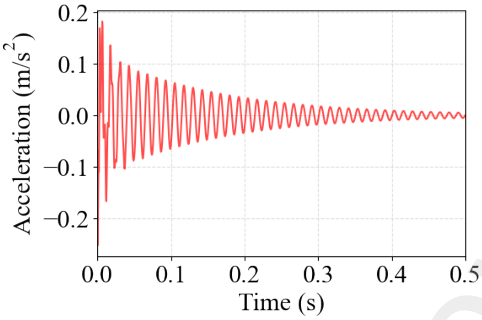


**Fig. 10.** Example of FE simulation data (Ch. 6, impact at Loc. 1)

Another detailed comparison between the measurement and simulation data in both time and frequency domains is shown in Fig. 11. The data are the vibration at Ch. 8 excited by the hammer impact at Loc. 8. In the time domain, the apparent differences in natural frequencies, amplitudes, and phases are qualitatively displayed. In the frequency domain, the difference in natural frequencies can be quantitively analysed, as summarized in Table 3. Observing the natural frequencies and damping ratios in Table 1, the differences between the measurement and simulation data can even reach 153.8%. Note that, no FE model updating was performed to minimize these differences, because we intended to investigate whether the proposed data synthesis method requests a precise FE model, or whether the proposed method can have great performance with a highly inaccurate FE model.

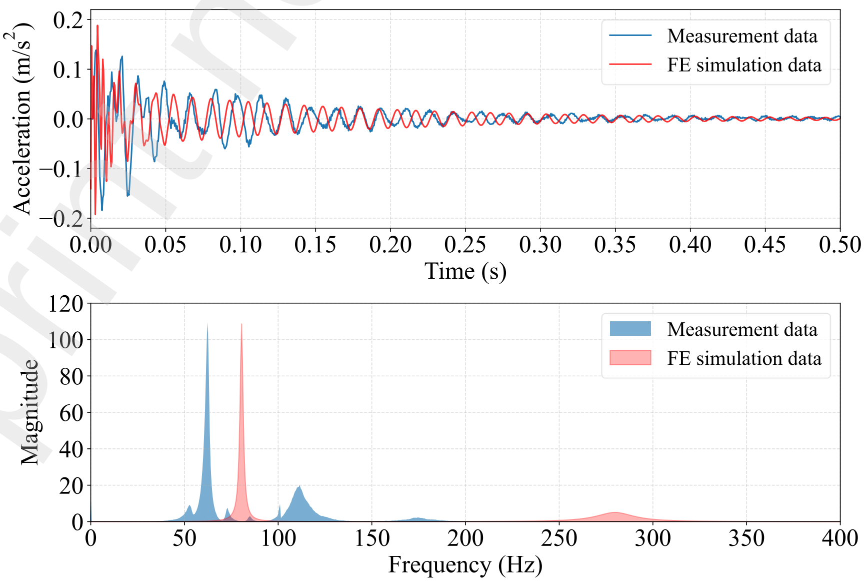


**Fig. 11.** Comparison between the measurement data and FE simulation data (Impact at Loc. 8, Ch. 8)

**Table 3.** Comparison between dynamic characteristics of the measurement and simulation data shown in Fig. 11

| Mode | Natural Frequency (Meas.) | Natural Frequency (Sim.) | Difference (ratio) | Damping Ratio (Meas.) | Damping Ratio (Sim.) | Difference (ratio) |
|---|---|---|---|---|---|---|
| 1 | 62.5 Hz | 80.5 Hz | 18 Hz (28.8%) | 2.15% | 1.26% | 0.89% (41.4%) |
| 2 | 110.5 Hz | 280.5 Hz | 170 Hz (153.8%) | 4.42% | 4.39% | 0.03% (0.68%) |

### *3.3. Network training scenarios*

Two training cases are tested for the proposed DCCNN with different amounts of training and validation data, as shown in Table 4. Case 1 is the scenario with sufficient training data, and Case 2 represents the scenario when only limited training data are available. In both cases, the vibration data excited by the impact loads at Locs. 5-8 were only used for test purposes. The difference between the two cases is the amount of training and validation data: Case 1 uses the data excited by the impact loads at Locs. 1-4 for training and validation, while Case 2 uses the data excited by the impact loads at only Loc. 1. The reason for choosing the data with impact only at Loc. 1 in Case 2 is that the impact loads near supports may lead to more complex vibration than the impacting other places. The numbers of training data in the two cases differ 3.5 times. The data split in Case 1 is used for the determination of the structure of the DCCNN, and Case 2 is for testing the performance of the DCCNN with limited training data.

**Table 4.** Data split in each case

| Case | Number of training data | Ratio (%) | Number of validation data | Ratio (%) | Number of test data | Ratio (%) |
|---|---|---|---|---|---|---|
| 1 | 636 (Locs. 1-4) | 49.8 | 71 (Locs. 1-4) | 5.6 | 570 (Locs. 5-8) | 44.6 |
| 2 | 180 (Loc. 1) | 23.4 | 21 (Loc. 1) | 2.7 | 570 (Locs. 5-8) | 73.9 |

The optimizer is Adam [61] and the loss function is MSE as defined in Eq. (1). All the DCCNNs were trained for 5000 epochs. The learning rate was initialized with 0.001, and the learning rate was scaled by a factor of 0.75 if the training loss did not reduce in 50 epochs. The results of Cases 1 and 2 are analysed and discussed in Section 4.

$$MSE = \frac{1}{n}\sum_{i=1}^{n} \left(y_i - y_i'\right)^2 \tag{1}$$

## 4. Results

This section discusses the results of data synthesis generated by the proposed DCCNN in the two training cases. By performing the vibration experiment and the FE simulation as introduced in

Section 3, two paired datasets, named measurement dataset and FE simulation dataset, are established for training, validating, and testing the proposed data synthesis method.

### *4.1. Results of Case 1*

As introduced in Table 5, the data with hammer impact at Locs. 1-4 were utilized for training and validation, and the rest data with hammer impact at Locs. 5-8 were used for testing. Fig. 12 shows the training procedures of the proposed DCCNN. Both training and validation losses decreased smoothly, and very low training and validation losses were finally achieved. No overfitting occurred during the training procedure.

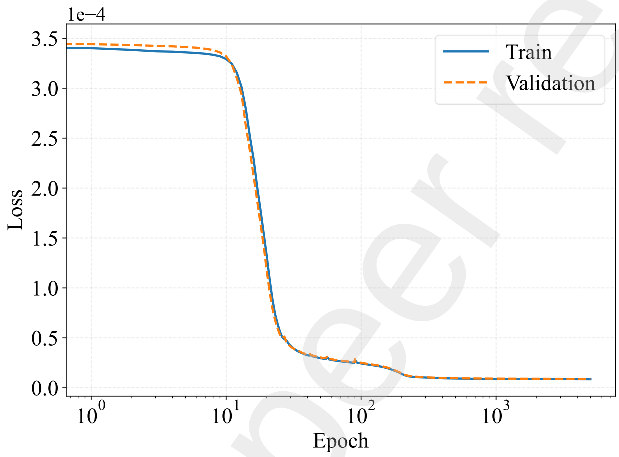


**Fig. 12.** Training history of Cases 1

To test the performance of the DCCNN model, the MSE of each test result is visualized in Fig. 13, which calculates the MSE between the measurement data (ground truth) and the synthetic data generated by the DCCNN. The MSE of each individual test data is in a range between 0.002 to 0.014, and the mean MSE is 0.006 for the whole test set, which exhibits the high fidelity of the synthetic data. The test data can be divided into 4 groups according to their impact locations (Locs. 5-8) by using different colours. Fig. 13 shows a phenomenon that, with relatively sufficient training data, the synthetic vibration data excited by the impact loads, that are close to the midpoint of the beam, tend to yield higher accuracy. In contrast, the synthetic vibration data excited by the impact loads, that are near to supports of the beam, tend to show a higher error. One possible reason for this phenomenon is the imperfect boundary conditions of the beam. When the impact load gets closer to the supports of the beam, the vibration tends to be more complex. As a result, the DCCNN is relatively more difficult to learn the features for synthetic data when the impact loads are close to the supports.

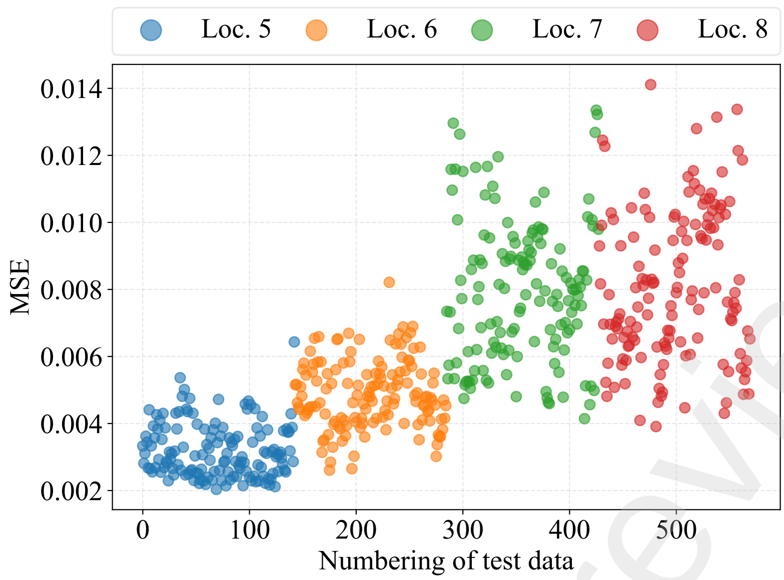


**Fig. 13.** MSE of each test data in Case 1 with the mean value of 0.006

Figs. 14 and 15 demonstrate the test result of the synthetic data generated by the proposed DCCNN in the Case 1 training scenario. Two data examples, which have lower and higher MSEs than the mean MSE of the whole test set 0.006, are randomly chosen from the test set. The first example shown in Fig. 14 is excited by an impact load at Loc. 5, and its MSE is 0.0034. The second example shown in Fig. 15 is excited by an impact load at Loc. 8, and the corresponding MSE is 0.0066. In the two figures, all 9 channels of the synthetic data and the corresponding measurement data are compared individually. In Fig. 14 the amplitude, phase, and frequency of the synthetic data precisely match the measurement data. In Fig. 15, the amplitudes of the first several periods of the synthetic data can be slightly lower than that of the measurement data. The frequency and phase are presented correctly. The results demonstrate that the proposed method can successfully synthesize the vibration data excited by the loads that are not involved in the training and validation process.

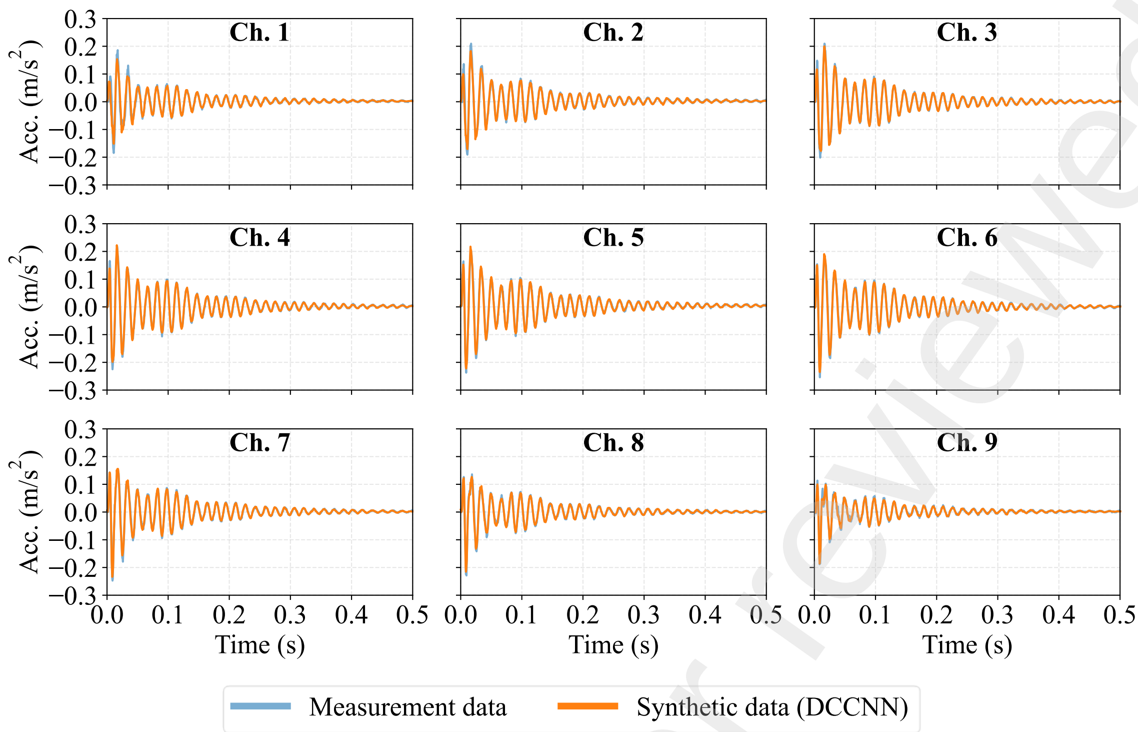


**Fig. 14.** Synthetic data generated by DCCNN (Case 1, impact on Loc. 5, MSE of 0.0034)

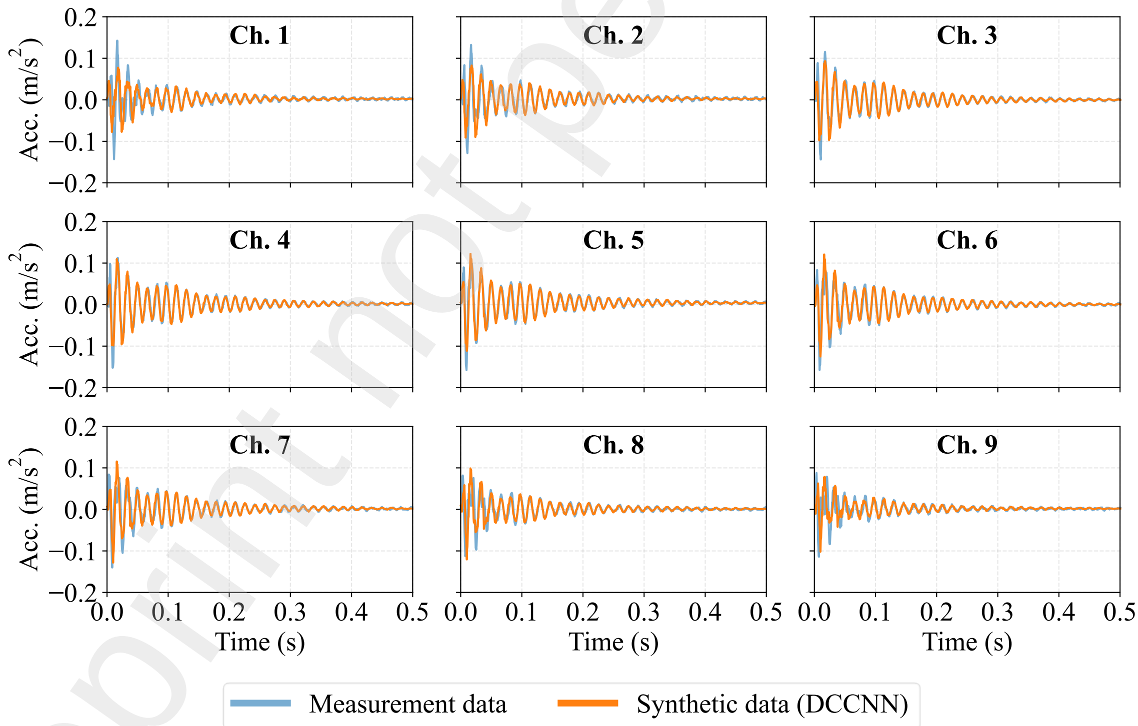


**Fig. 15.** Synthetic data generated by DCCNN (Case 1, impact at Loc.8, MSE of 0.0066)

To view more details of the synthetic data, Fig. 16 visualises the first 0.1 s of Ch. 5 in Fig. 14. Comparing the synthetic data and the corresponding measurement data (ground truth), the synthetic data precisely represent the low-frequency components of the measurement data. The difference in the high-frequency components between the measurement and synthetic data can be observed. The waveform of the measurement data has apparent sawteeth, but the waveform of the DCCNN synthesised data is smoother, indicating fewer high-frequency components in the synthetic data. Such a characteristic of DCCNN makes it feasible to have the additional function of a smoother or low-pass filter.

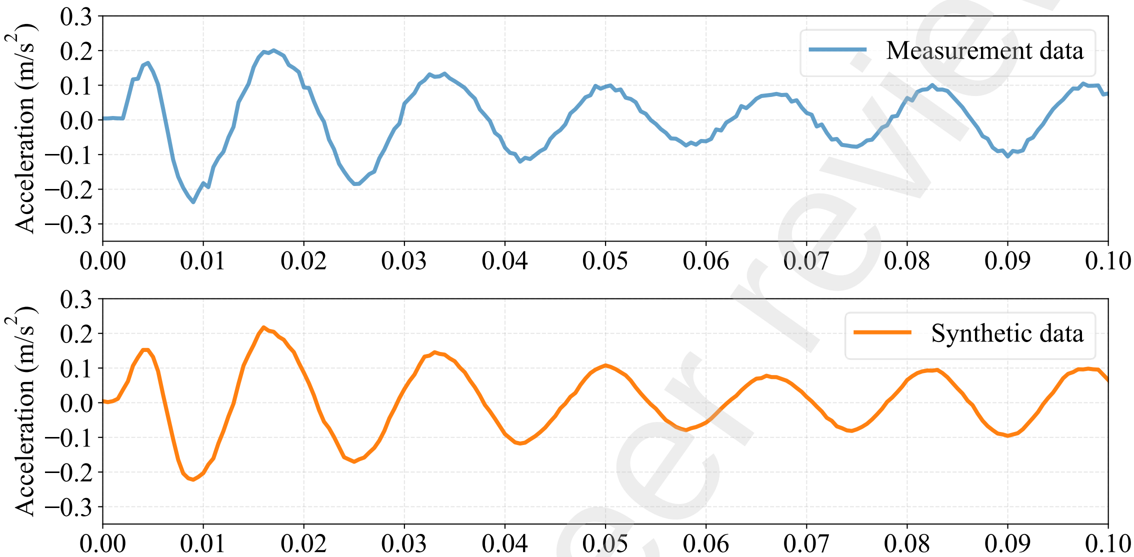


**Fig. 16.** First 0.1 s of the Ch. 5 in the synthetic data shown in Fig. 14

Subsequently, to investigate the quality of the synthetic data from the frequency perspective, we performed Fast Fourier Transformation (FFT) on the FE simulation, measurement, and synthetic data. Ch. 9 of the example (shown in Fig. 14) was visualised in Fig. 17. The subplots in the first row are the time-series waveforms, the subplots in the second row are the FFT spectrums in a linear scale, and the subplots in the last row are the FFT spectrums in the dB scale. From the linear-scale spectrums of the measurement data and synthetic data, two dominant peaks at 62.5 Hz and 110.5 Hz can be detected, indicating accurate representations of the natural modes of the beam in the synthetic data. In the dB-scale spectrum of synthetic data, the magnitudes over 200 Hz are lower than the corresponding measurement data, which proves that DCCNN has the characteristics of low-pass filter, and the components higher than about 200 Hz are depressed.

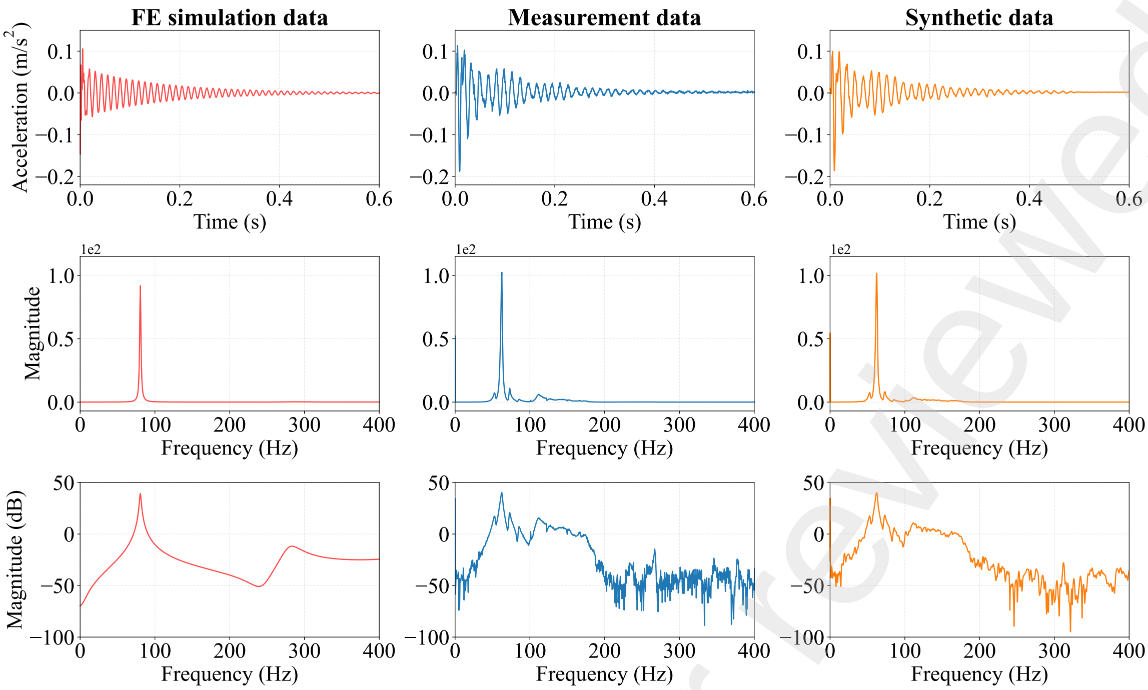


**Fig. 17.** Comparison of FE simulation, measurement, and synthetic data in the frequency domain (impact at Loc. 5, Ch. 9 of the data example in Fig. 14)

Furthermore, the mode shapes of the first two bending modes are identified from each synthetic and measurement data in the test set using cross spectrum method. The mean mode shapes of the test set data are calculated and visualised in Fig. 18, in which the mean mode shapes identified from the synthetic data are highly consistent with those of the measurement data. Even though the measured mode shapes are apparently different from simulation results, the proposed DCCNN can accurately reproduce the mode shape information in the synthetic data. Modal Assurance Criterion (MAC), as defined in Eq. (2), is used as an indicator to quantitively evaluate the accuracy of the mode shapes identified from the synthetic data. The MACs of the synthetic, FE simulation, and measurement data are analysed and visualized in Fig. 19. Overall, the MAC values of the mean mode shapes identified from the synthetic data are greater than 0.9742 compared to those of the measurement data, indicating the high quality of the synthetic data generated by the DCCNN.

$$MAC(\varphi_A,\varphi_B) = \frac{|\{\varphi_A\}^T\{\varphi_B\}|^2}{(\{\varphi_A\}^T\{\varphi_A\})(\{\varphi_B\}^T\{\varphi_B\})} \tag{2}$$

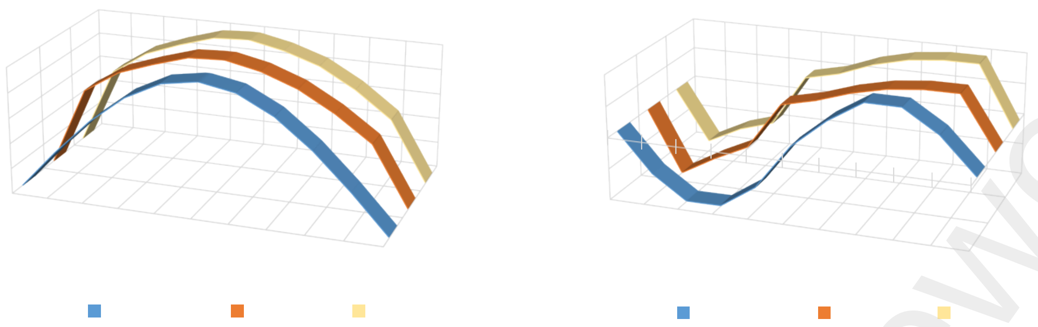

(a) (b)

**Fig. 18.** Mean mode shapes identified from the synthetic data generated in Case 1. (a) Mode 1, 1st bending mode, (b) Mode 2, 2nd bending mode.

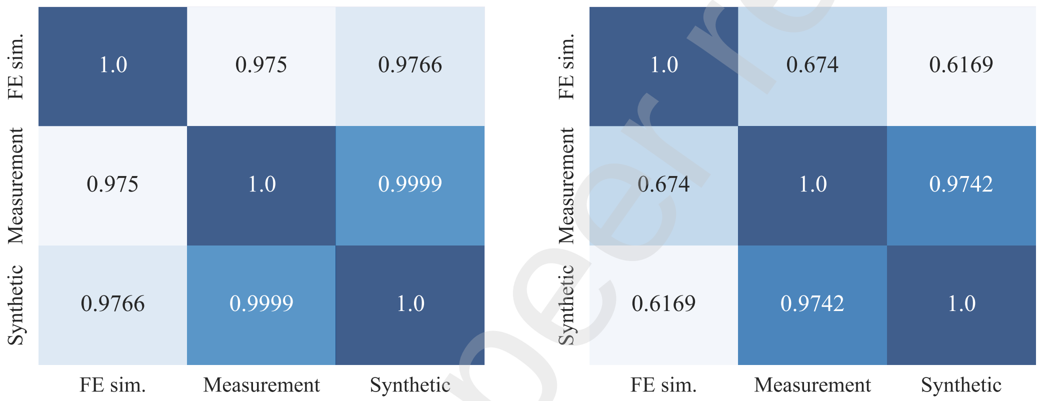


(a) (b)

**Fig. 19.** MAC of mean mode shapes in Case 1. (a) Mode 1, (b) Mode 2

### *4.2. Results of Case 2*

As obtaining sufficient training data is very difficult or even impossible in many actual engineering scenarios, training with a small scale of data has become a natural need for DL modelling. To investigate the performance of the proposed DCCNN under the training scenario with limited data, in this section, only 180 data with impact at Loc. 1 are used for training, other 21 data with impact at Loc. 1 are for validation, and the data with impact at Locs. 5-8 are for testing.

The training histories of losses in Case 2 are shown in Fig. 20. The training loss and validation loss were reduced smoothly and simultaneously. No overfitting appeared in the training procedures. Finally, the losses reached a $10^{-5}$ level, which indicates that the models have learned critical features from the measurement data.

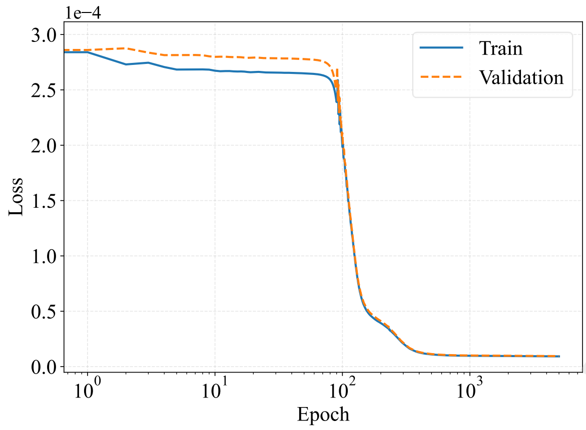


**Fig. 20.** Training history of Case 2

To test the performance of the DCCNN model trained with limited data, the MSE of each test result is visualized in Fig. 21, which calculates the MSE between the measurement data (ground truth) and the synthetic data generated by the DCCNN. The MSE of each individual test data is in a range between 0.004 to 0.028, and the mean MSE of the whole test set is 0.014. Interestingly, comparing the test results of Case 2 to Case 1, the number of training data in Case 2 is only 28.39% of it in Case 1. However, the lower bound, upper bound, and the mean value of the test errors in Case 2 are approximately doubled. The test errors in Case 2 are not greatly affected by the sudden reduction of training data. Fig. 21 also shows a phenomenon that, only using the data with impact at Loc. 1 for training, the MSEs of the synthetic data with impact at Locs. 5-7 are generally in the same range, and the MSEs of the synthetic data with impact at Loc. 8 are apparently lower than those of Locs. 5-7. One possible explanation for this phenomenon is that the DCCNN has only learned the features of the vibration excited by the loads close to the support (Loc. 1). Since Loc.8 is also close to the support, and it is in the symmetric position of Loc. 1, better test results were obtained when the impacts are in Loc. 8 of the test data.

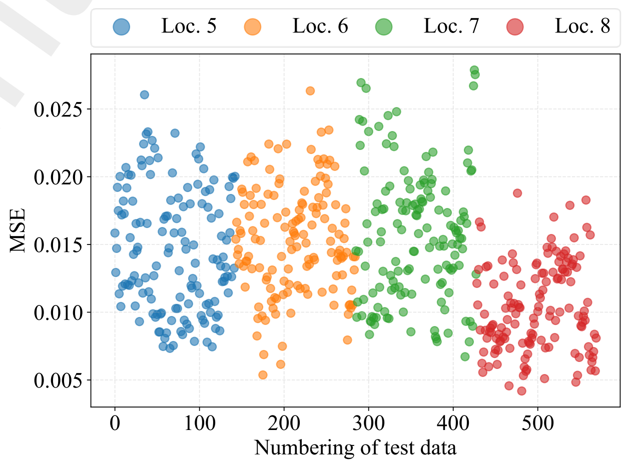


**Fig. 21.** MSE of each test data in Case 2 with the mean value of 0.014

Figs. 22 and 23 demonstrate the two examples of the synthetic data in the test set, which are generated by the proposed DCCNN trained with limited data in Case 2. The two test data are the two used in Figs. 14 and 15. The MSEs of the two test examples are 0.0159 and 0.0081, which are higher and lower than the mean MSE of the whole test set (0.014), respectively. Observing Figs. 22 and 23, when trained with limited data, even though the amplitudes of the synthetic data are not as accurate as those in Figs. 14 and 15 in Case 1, the DCCNN can successfully learn the dominant features of the vibration, like frequencies and phases.

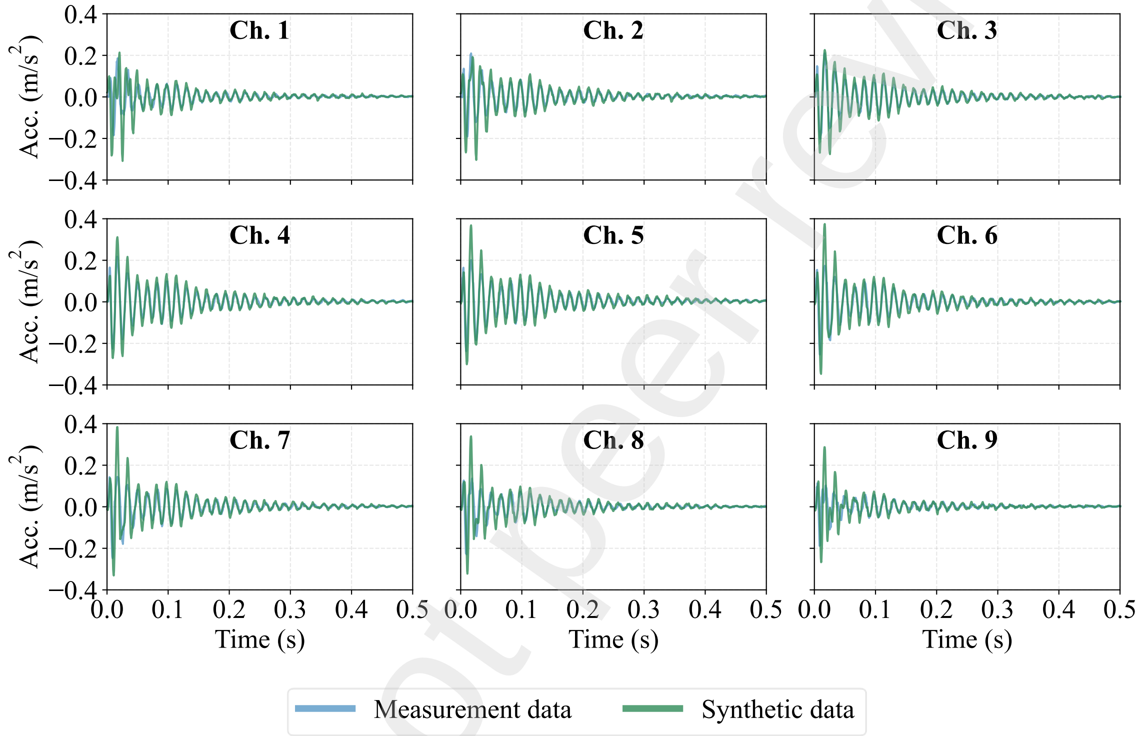


**Fig. 22.** Synthetic data generated by DCCNN (Case 2, impact at Loc. 5, MSE of 0.0159)

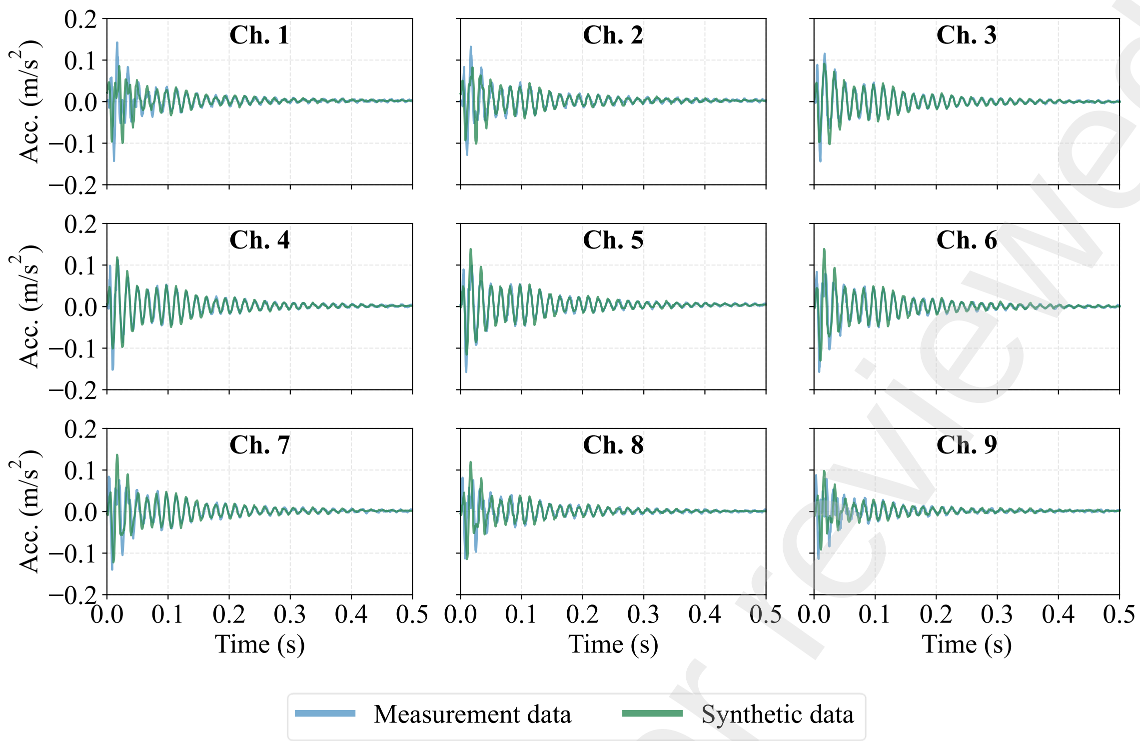


**Fig. 23.** Synthetic data generated by DCCNN (Case 2, impact at Loc.8, MSE of 0.0081)

Then, to investigate the quality of the synthetic data in the frequency domain, we performed FFT on the FE simulation, measurement, and synthetic data. Using Ch. 6 in Fig. 23 as an example, as visualised in Fig. 24, the subplots of waveforms in the first row show the amplitudes of the synthetic data lose some accuracy with the reduction of training data. In the FFT subplots in the second and third rows, the two peaks indicate the synthetic data can successfully reproduce the mode features. In the dB-scale spectrum of synthetic data, the magnitudes over 100 Hz show also lower accuracy than the corresponding measurement data, which proves that DCCNN has the characteristics of low-pass filter, and the components higher than about 100 Hz are depressed.

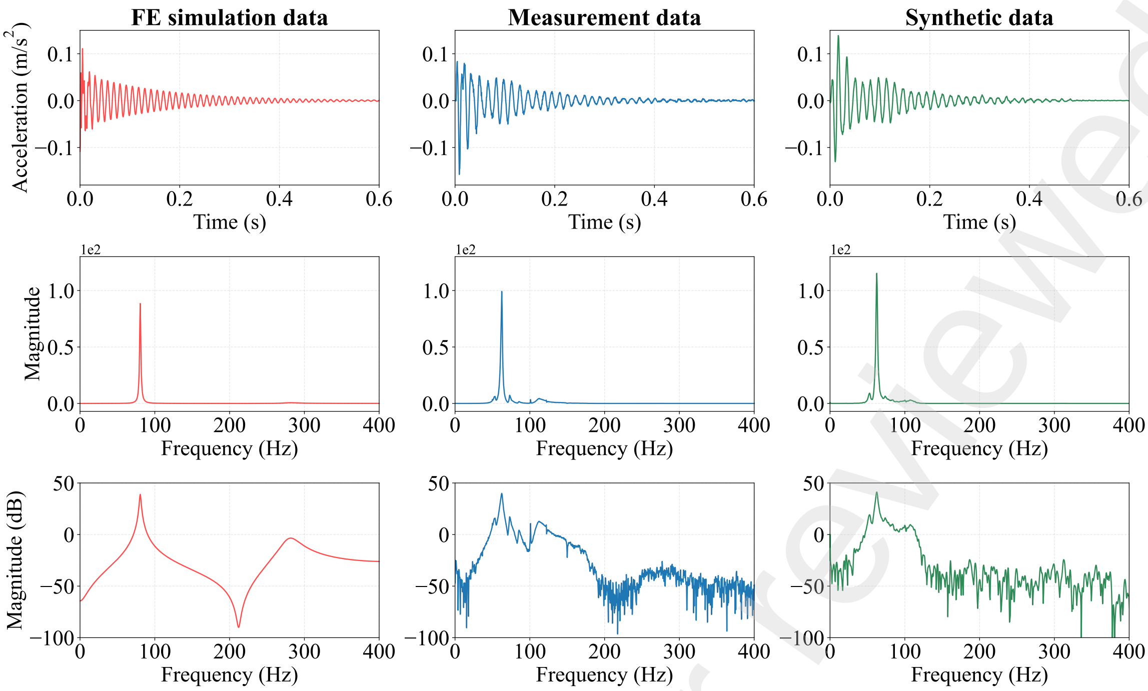


**Fig. 24.** Comparison of FE simulation, measurement, and synthetic data in the frequency domain (impact at Loc. 8, Ch. 6 of the data example in Fig. 23)

Meanwhile, the accuracies of the mean mode shapes identified from the synthetic data in the test set of Case 2 are also analysed. Fig. 25 compares the identified mean mode shapes of the synthetic data in the whole test set to those of the FE simulation and measurement data. Both Modes 1 and 2 can be identified from the synthetic data. The consistencies of the identified mode shapes are shown in Fig. 26. The values of MAC for all the identified mode shapes are higher than 0.98, indicating the accurate representation of the proposed networks even with limited training data.

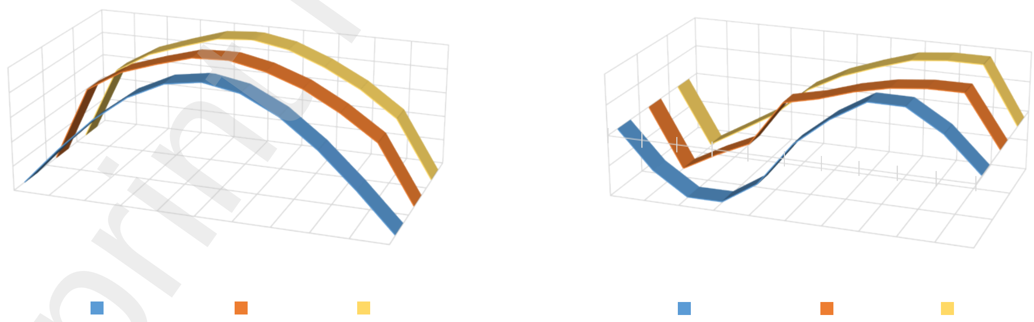

(a) (b)

**Fig. 25.** Mode shapes identified from the synthetic data generated in Case 1. (a) Mode 1: 1$^{st}$ bending mode, (b) Mode 2: 2$^{nd}$ bending mode.

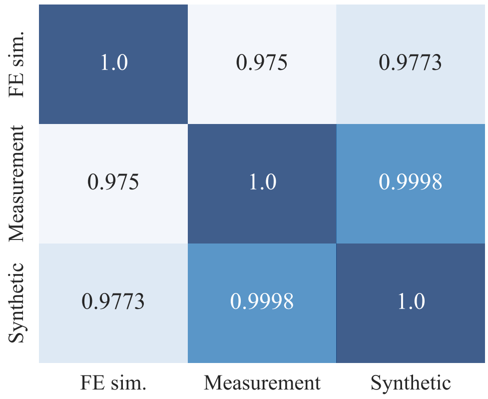


(a)

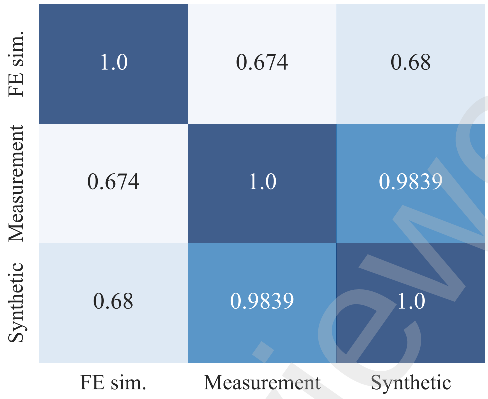


(b)

**Fig. 26.** MAC of mode shapes in Case 2. (a) Mode 1, (b) Mode 2

## 5. Conclusions

In this paper, we proposed a novel method to synthesise high-fidelity time-series data. The proposed method consists of experiments, FE simulation, and space projection using DL. Low-fidelity FE simulation data can be transferred to high-fidelity measurement data in an end-to-end manner. A DL model DCCNN was designed for this projecting task. Both physical and numerical vibration experiments were performed to test the proposed method. The remarkable quality of the synthetic data demonstrates the effectiveness of the proposed method. Some detailed conclusions are drawn as follows.

First, the proposed method can accurately synthesise the vibration data excited by the loads that were not used for training and validation. This shows the applicability of the proposed method for synthesising high-fidelity structural dynamics when the desired loads are not available or cannot be applied on real structures.

Second, the proposed method can generate realistic synthetic vibration data of structures without performing FE model updating. Compared to the measurement data acquired directly from the structure, the synthetic vibration data are very accurate when observed in the time domain, frequency domain, natural frequencies, phase, amplitude, and mode shapes. The high-quality synthetic data also indicates the rationality of the design of the DCCNN for the data synthesis task.

Third, the proposed DCCNN has the characteristics of low-pass filter. When in the normal training case with sufficient training data, DCCNN tends to depress the components higher than 200 Hz. When training with limited data, the DCCNN tends to depress the components higher than 100 Hz. Such a feature makes the DL models can be considered with an integrated noise reducer.

The proposed method can contribute to all the downstream tasks, for instance, analyses of structural dynamic behaviours, design optimisation, data-driven identification tasks, etc., which request time-series simulation data. Our future work will be focused on addressing the following limitations. First, the performance of the proposed data synthesis method with other types of loads and structural responses is unknown. Excitations with actuators and forced vibration data will be used to further test and update the proposed method. Second, the DCCNN needs to be slightly refined when the structure and corresponding FE model are changed. Our next work includes the development of a method to model the domain shift and avoid the data required for refining the DCCNN when the structure and FE model are changed. This aims to synthesise dynamic responses of the structure with specified non-existent changes or damage.

## CRediT author statement

**Youqi Zhang:** Conceptualization, Methodology, Software, Formal analysis, Investigation, Validation, Resources, Data Curation, Writing - Original Draft, Visualization, Funding acquisition. **Zhenkun Li:** Software, Formal analysis. **Rui Hao:** Investigation. **Weiwei Lin:** Resources, Funding acquisition. **Lingfang Li:** Software, Formal analysis. **Di Su:** Funding acquisition. All the authors reviewed and edited the manuscript.

## Declaration of competing interest

The authors declare that they have no known competing financial interests or personal relationships that could have appeared to influence the work reported in this paper.

## Acknowledgment

The authors greatly acknowledge the financial support from the Academy of Finland (decision number: 339493). The 2nd and 4th authors are financially supported by the Jane and Aatos Erkko Foundation in Finland. The assistance of the laboratory staff at Aalto University is also gratefully acknowledged.

## References

[1] L. Lombardi, F. De Luca, J. Macdonald, Design of buildings through linear time-history analysis optimising ground motion selection: a case study for RC-MRFs, Engineering Structures, 192 (2019) 279-295.
[2] C. Jin, W.C. Chung, D.-S. Kwon, M. Kim, Optimization of tuned mass damper for seismic control of submerged floating tunnel, Engineering Structures, 241 (2021) 112460.
[3] G. He, D. Cao, Y. Cao, W. Huang, Dynamic modeling and orbit maneuvering response analysis for a three-axis attitude stabilized large scale flexible spacecraft installed with hinged solar arrays, Mechanical Systems and Signal Processing, 162 (2022) 108083.
[4] T.R. Felipe, A.T. Beck, Dynamic analysis of failure paths of truss structures: Benchmark examples including material degradation, Mechanical Systems and Signal Processing, 158 (2021) 107767.
[5] Z. Yang, Y. Li, H. Guan, M. Diao, B.P. Gilbert, H. Sun, L. Xu, Dynamic response and collapse resistance of RC flat plate structures subjected to instantaneous removal of an interior column, Engineering Structures, 264 (2022) 114469.
[6] J. Liu, P. Wang, X. Guo, L. Dai, Y. He, Nonlinear vibration model and response characteristic of drilling risers in deep-sea under soft suspension evacuation condition, Mechanical Systems and Signal Processing, 169 (2022) 108783.

[7] C. Yeung, C.T. Ng, Time-domain spectral finite element method for analysis of torsional guided waves scattering and mode conversion by cracks in pipes, Mechanical Systems and Signal Processing, 128 (2019) 305-317.
[8] L. Li, M. Faisal Haider, H. Mei, V. Giurgiutiu, Y. Xia, Theoretical calculation of circular-crested Lamb wave field in single-and multi-layer isotropic plates using the normal mode expansion method, Structural Health Monitoring, 19 (2020) 357-372.
[9] D. Su, Y. Fujino, T. Nagayama, J.Y. Hernandez, M. Seki, Vibration of reinforced concrete viaducts under high-speed train passage: measurement and prediction including train–viaduct interaction, Structure and Infrastructure Engineering, 6 (2010) 621-633.
[10] Y.z. Lin, Z.h. Nie, H.w. Ma, Structural damage detection with automatic feature-extraction through deep learning, Computer-Aided Civil and Infrastructure Engineering, 32 (2017) 1025-1046.
[11] T. Guo, L. Wu, C. Wang, Z. Xu, Damage detection in a novel deep-learning framework: a robust method for feature extraction, Structural Health Monitoring, 19 (2020) 424-442.
[12] P. Seventekidis, D. Giagopoulos, A. Arailopoulos, O. Markogiannaki, Structural Health Monitoring using deep learning with optimal finite element model generated data, Mechanical Systems and Signal Processing, 145 (2020) 106972.
[13] Y.B. Yang, B. Zhang, Y. Qian, Y. Wu, Contact-Point Response for Modal Identification of Bridges by a Moving Test Vehicle, International Journal of Structural Stability and Dynamics, 18 (2017) 1850073.
[14] D.A. Ramatlo, C.S. Long, P.W. Loveday, D.N. Wilke, Physics-based modelling and simulation of reverberating reflections in ultrasonic guided wave inspections applied to welded rail tracks, Journal of Sound and Vibration, 530 (2022) 116914.
[15] C. Boller, Chang, F. K., & Fujino, Y. (Eds.). , Encyclopedia of structural health monitoring, Wiley Online Library, 2009.
[16] L. Sun, Z. Shang, Y. Xia, S. Bhowmick, S. Nagarajaiah, Review of bridge structural health monitoring aided by big data and artificial intelligence: From condition assessment to damage detection, Journal of Structural Engineering, 146 (2020) 04020073.
[17] T. Khuc, T.A. Nguyen, H. Dao, F.N. Catbas, Swaying displacement measurement for structural monitoring using computer vision and an unmanned aerial vehicle, Measurement, 159 (2020) 107769.
[18] M. Sanayei, A. Khaloo, M. Gul, F.N. Catbas, Automated finite element model updating of a scale bridge model using measured static and modal test data, Engineering Structures, 102 (2015) 66-79.
[19] A. Öchsner, M. Merkel, One-Dimensional Finite Elements, Springer, 2013.
[20] J.N. Reddy, Introduction to the finite element method, McGraw-Hill Education, 2019.
[21] F. Hartmann, C. Katz, Structural analysis with finite elements, Springer Science & Business Media, 2004.
[22] H. Salehi, R. Burgueño, Emerging artificial intelligence methods in structural engineering, Engineering structures, 171 (2018) 170-189.
[23] R.B. Corotis, An overview of uncertainty concepts related to mechanical and civil engineering, ASCE-ASME Journal of Risk and Uncertainty in Engineering Systems Part B: Mechanical Engineering, 1 (2015) 040801.
[24] Y. Bao, Z. Tang, H. Li, Y. Zhang, Computer vision and deep learning–based data anomaly detection method for structural health monitoring, Structural Health Monitoring, 18 (2019) 401-421.
[25] Y. Zhang, Z. Tang, R. Yang, Data anomaly detection for structural health monitoring by multi-view representation based on local binary patterns, Measurement, 202 (2022) 111804.
[26] E. Simoen, G. De Roeck, G. Lombaert, Dealing with uncertainty in model updating for damage assessment: A review, Mechanical Systems and Signal Processing, 56 (2015) 123-149.
[27] M. Machado, S. Adhikari, J. Dos Santos, J. Arruda, Estimation of beam material random field properties via sensitivity-based model updating using experimental frequency response functions, Mechanical Systems and Signal Processing, 102 (2018) 180-197.

[28] S. Sehgal, H. Kumar, Structural dynamic model updating techniques: a state of the art review, Archives of Computational Methods in Engineering, 23 (2016) 515-533.
[29] H.-P. Chen, T.S. Maung, Regularised finite element model updating using measured incomplete modal data, Journal of Sound and Vibration, 333 (2014) 5566-5582.
[30] A. Mojtahedi, H. Hokmabady, A. Yaghubzadeh, S. Mohammadyzadeh, An improved model reduction-modal based method for model updating and health monitoring of an offshore jacket-type platform, Ocean Engineering, 209 (2020) 107495.
[31] W. Zhao, L. Yang, C. Dang, R. Rocchetta, M. Valdebenito, D. Moens, Enriching stochastic model updating metrics: An efficient Bayesian approach using Bray-Curtis distance and an adaptive binning algorithm, Mechanical Systems and Signal Processing, 171 (2022) 108889.
[32] B. Goller, G. Schueller, Investigation of model uncertainties in Bayesian structural model updating, Journal of sound and vibration, 330 (2011) 6122-6136.
[33] J. Jang, A. Smyth, Bayesian model updating of a full-scale finite element model with sensitivity-based clustering, Structural Control and Health Monitoring, 24 (2017) e2004.
[34] A. Esfandiari, An innovative sensitivity-based method for structural model updating using incomplete modal data, Structural Control and Health Monitoring, 24 (2017) e1905.
[35] M. Rezaiee-Pajand, A. Entezami, H. Sarmadi, A sensitivity-based finite element model updating based on unconstrained optimization problem and regularized solution methods, Structural Control and Health Monitoring, 27 (2020) e2481.
[36] S. Cong, S.-L.J. Hu, H.-J. Li, FRF-based pole-zero method for finite element model updating, Mechanical Systems and Signal Processing, 177 (2022) 109206.
[37] M.H. Jalali, D.G. Rideout, Frequency-based decoupling and finite element model updating in vibration of cable–beam systems, Journal of Vibration and Control, 28 (2022) 1520-1535.
[38] T. Marwala, Finite-element-model updating using computional intelligence techniques: Applications to structural dynamics, Springer, 2010.
[39] P. Noever-Castelos, D. Melcher, C. Balzani, Model updating of a wind turbine blade finite element Timoshenko beam model with invertible neural networks, Wind Energy Science, 7 (2022) 623-645.
[40] J. Jung, H. Jun, P.-S. Lee, Self-updated four-node finite element using deep learning, Computational Mechanics, 69 (2022) 23-44.
[41] J. Naranjo-Pérez, M. Infantes, J.F. Jiménez-Alonso, A. Sáez, A collaborative machine learning-optimization algorithm to improve the finite element model updating of civil engineering structures, Engineering Structures, 225 (2020) 111327.
[42] I. Goodfellow, Y. Bengio, A. Courville, Deep learning, MIT press, 2016.
[43] Y. LeCun, Y. Bengio, G. Hinton, Deep learning, nature, 521 (2015) 436-444.
[44] X. Ye, T. Jin, C. Yun, A review on deep learning-based structural health monitoring of civil infrastructures, Smart Struct. Syst, 24 (2019) 567-585.
[45] Y. Bao, Z. Chen, S. Wei, Y. Xu, Z. Tang, H. Li, The state of the art of data science and engineering in structural health monitoring, Engineering, 5 (2019) 234-242.
[46] R. Zhao, R. Yan, Z. Chen, K. Mao, P. Wang, R.X. Gao, Deep learning and its applications to machine health monitoring, Mechanical Systems and Signal Processing, 115 (2019) 213-237.
[47] Y.J. Cha, W. Choi, O. Büyüköztürk, Deep learning-based crack damage detection using convolutional neural networks, Computer-Aided Civil and Infrastructure Engineering, 32 (2017) 361-378.
[48] Y.J. Cha, W. Choi, G. Suh, S. Mahmoudkhani, O. Büyüköztürk, Autonomous structural visual inspection using region-based deep learning for detecting multiple damage types, Computer-Aided Civil and Infrastructure Engineering, 33 (2018) 731-747.
[49] C.-Z. Dong, F.N. Catbas, A review of computer vision–based structural health monitoring at local and global levels, Structural Health Monitoring, 20 (2021) 692-743.
[50] O. Abdeljaber, O. Avci, M.S. Kiranyaz, B. Boashash, H. Sodano, D.J. Inman, 1-D CNNs for structural damage detection: Verification on a structural health monitoring benchmark data, Neurocomputing, 275 (2018) 1308-1317.
[51] Y. Zhang, Y. Miyamori, S. Mikami, T. Saito, Vibration-based structural state identification by a 1-dimensional convolutional neural network, Computer-Aided Civil and Infrastructure Engineering, 34 (2019) 822-839.

[52] O. Abdeljaber, O. Avci, S. Kiranyaz, M. Gabbouj, D.J. Inman, Real-time vibration-based structural damage detection using one-dimensional convolutional neural networks, Journal of Sound and Vibration, 388 (2017) 154-170.
[53] X. Hou, Y. Zeng, J. Xue, Detecting structural components of building engineering based on deep-learning method, Journal of Construction Engineering and Management, 146 (2020) 04019097.
[54] Y. Zhang, Z. Li, R. Hao, W. Lin, L. Li, D. Su, Vibration Data Synthesis by using Finite Element Analysis and Artificial Neural Network, 8th World Conference on Structural Control and Monitoring (8WCSCM), IASCM Orlando, Florida, USA, 2022.
[55] Y. LeCun, A theoretical framework for back-propagation, Proceedings of the 1988 connectionist models summer school, 1988, pp. 21-28.
[56] A. Van Den Oord, S. Dieleman, H. Zen, K. Simonyan, O. Vinyals, A. Graves, N. Kalchbrenner, A.W. Senior, K. Kavukcuoglu, WaveNet: A generative model for raw audio, SSW, 125 (2016) 2.
[57] D. Rethage, J. Pons, X. Serra, A wavenet for speech denoising, 2018 IEEE International Conference on Acoustics, Speech and Signal Processing (ICASSP), IEEE, 2018, pp. 5069-5073.
[58] A. Oord, Y. Li, I. Babuschkin, K. Simonyan, O. Vinyals, K. Kavukcuoglu, G. Driessche, E. Lockhart, L. Cobo, F. Stimberg, Parallel wavenet: Fast high-fidelity speech synthesis, International conference on machine learning, PMLR, 2018, pp. 3918-3926.
[59] Y. Lu, P. Xiang, P.-s. Dong, X. Zhang, J. Zeng, Analysis of the effects of vibration modes on fatigue damage in high-speed train bogie frames, Engineering Failure Analysis, 89 (2018) 222-241.
[60] X.-R. Huang, L. Jézéquel, S. Besset, L. Li, O. Sauvage, Nonlinear hybrid modal synthesis based on branch modes for dynamic analysis of assembled structure, Mechanical Systems and Signal Processing, 99 (2018) 624-646.
[61] D.P. Kingma, J. Ba, Adam: A method for stochastic optimization, arXiv preprint arXiv:1412.6980, (2014).